

1 *The paper is a non-peer reviewed preprint submitted to EarthArXiv.*

2 *The manuscript is presently under consideration at Earth and Planetary Science Letters.*

3

4

5 **Helium, carbon and nitrogen isotope evidence for slab influence on volcanic gas emissions**
6 **at Rabaul caldera, Papua New Guinea**

7 B.T. MCCORMICK KILBRIDE*¹, P.H. BARRY², T.P. FISCHER³, G. HOLLAND¹, M. HUDAK⁴, S. NOWICKI³,
8 C. BALLENTINE⁵, M. HÖHN¹, I. ITIKARAI⁶, K. MULINA⁶, E.J. NICHOLSON⁷

9 ¹Department of Earth Sciences, University of Manchester

10 ²Marine Chemistry and Geochemistry Department, Woods Hole Oceanographic Institution

11 ³Department of Earth and Planetary Sciences, University of New Mexico

12 ⁴Department of Geosciences, Williams College

13 ⁵Department of Earth Sciences, University of Oxford

14 ⁶Rabaul Volcanological Observatory

15 ⁷Department of Earth Sciences, University College London

16

17

18 *Corresponding author, brendan.mccormickkilbride@manchester.ac.uk (@BrendanVolc)

19

20 **Abstract**

21 The chemical and isotopic composition of the gases emitted by subduction zone volcanoes can provide
22 insights into the origin of magmatic volatiles. In volcanic arcs, magmatic volatiles and therefore
23 emitted gases can be supplied from the mantle, the subducting slab, or the rocks of the arc crust.
24 Determining the relative contributions of these distinct sources is important for understanding the
25 transfer of volatiles between Earth's interior and exterior reservoirs, which has implications for the
26 physical and chemical evolution of both the mantle and the atmosphere. Each subduction zone is a
27 different experiment in recycling efficiency according to the composition of the slab and the pressure-
28 temperature path it experiences on subduction, and accordingly all volcanic arc emissions can be
29 characterised by their particular chemical and isotopic compositions. In this study, we analyse the
30 composition of volcanic gases from Rabaul caldera in the New Britain subduction zone, Papua New
31 Guinea, and show that the emissions are substantially influenced by slab recycling of carbon and
32 nitrogen. We find helium emissions are dominated by a mantle contribution, with little influence from
33 the arc crust. Carbon isotopes point to a mixture of mantle, carbonate and organic sediment-derived
34 contributions, with carbonate dominant. This may be of sedimentary origin, seafloor calcareous muds,
35 or altered basalts of the subducting oceanic crust. Nitrogen isotopes also indicate a significant
36 influence of organic sediments. Our study is the first comprehensive investigation of volatile sources
37 in this subduction and our results and interpretation are consistent with previous studies of element
38 recycling based on New Britain arc lavas.

39

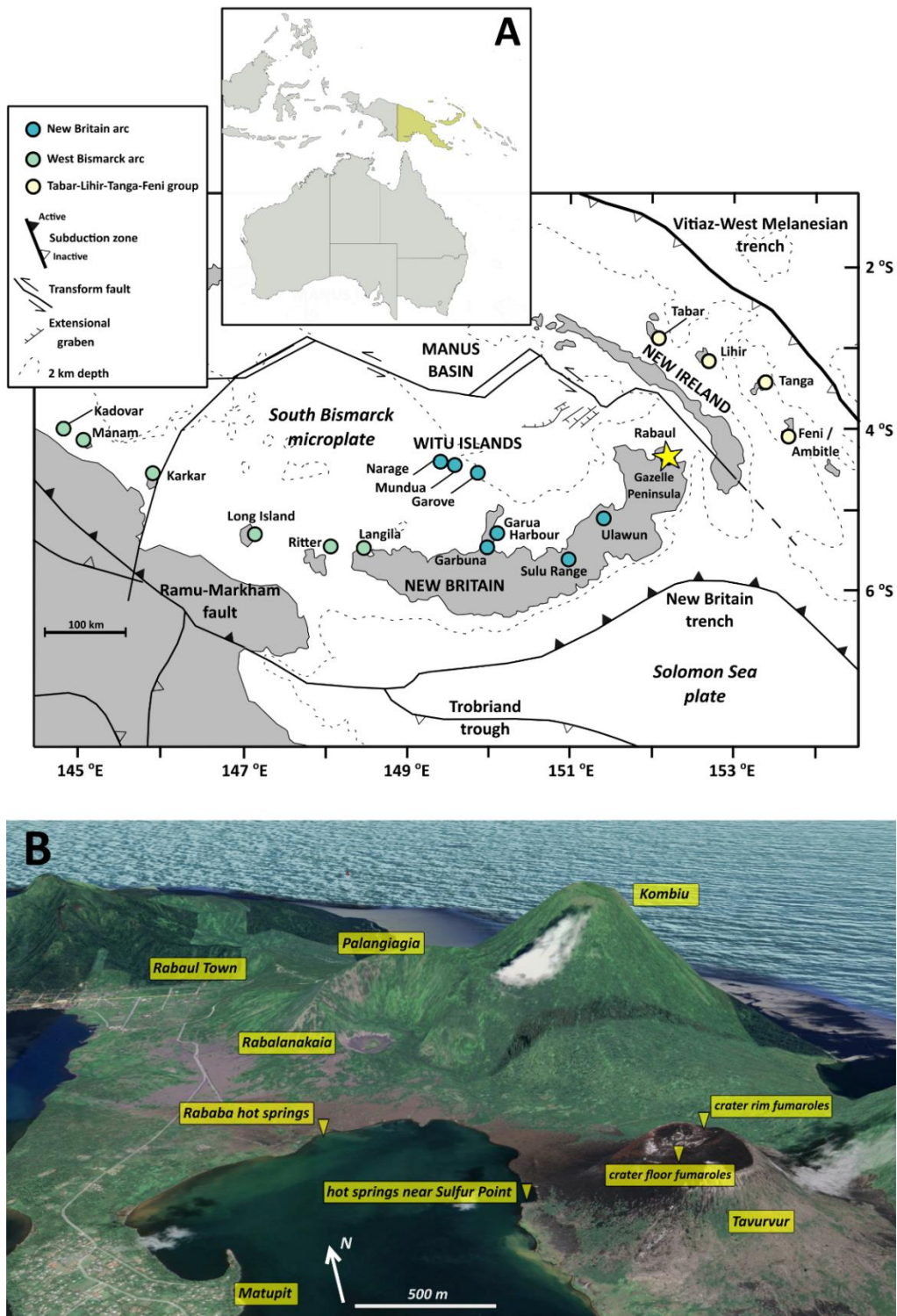
40

41 1. Introduction

42 Rabaul is a restless caldera volcano in East New Britain province, Papua New Guinea (PNG, Figure 1).
43 Since the last caldera forming eruption (667-699 CE), there have been numerous eruptions, of diverse
44 styles, from multiple intra-caldera vents (Bernard and Bouvet de Maisonneuve, 2020; Fabbro et al.,
45 2020; Heming, 1974; McKee et al., 2015; Patia et al., 2017; Wood et al., 1995). The most recent
46 eruptions (1994-2014) were accompanied by substantial outgassing from the caldera's most active
47 cone, Tavurvur (Carn et al., 2016; Global Volcanism Program, 2013; McCormick et al., 2012). Rabaul
48 has been cited as among the highest emitters of volcanic gas into the atmosphere over the past two
49 decades, the active cone of Tavurvur, where outgassing has been focussed, ranked seventh worldwide
50 for both SO₂ and CO₂ flux in 2005-2015 (Aiuppa et al., 2019; Carn et al., 2017). Following the cessation
51 of eruptive activity, unrest at Rabaul has dwindled to significantly lower levels, in terms of the intensity
52 of seismicity or ground deformation, vigour of gas emissions, and the temperature and overall
53 abundance of hot springs and fumaroles across the caldera. It remains unclear whether prodigious gas
54 emissions from Rabaul are an inherent characteristic of the volcanic system or a transient feature,
55 given the short history of instrumented monitoring. The chemical and isotopic composition of gas
56 emissions at Rabaul have been little studied and we do not know whether, or to what extent, volatiles
57 are supplied to the volcanic system from (i) the nearby subducting Solomon Sea plate or (ii) crustal
58 rocks of the New Britain volcanic arc. Magmatic volatiles play a key role in modulating eruption style
59 and intensity at Rabaul and understanding their origin and abundance is therefore critically important
60 for hazard assessment and risk mitigation (Bernard et al., 2022).

61 In this contribution, we present geochemical and isotopic data from volcanic gases at Rabaul, collected
62 from Tavurvur crater fumaroles and nearby hot springs in 2016 and 2019. We report the composition
63 of gases in terms of the relative abundance of major (H₂O, CO₂, sulfur) and trace (He, Ar, N₂) chemical
64 species, as well as helium, carbon, nitrogen and argon isotopes. These are valuable tracers for
65 determining the relative proportion of volatiles supplied from the mantle and the crust (Barry et al.,
66 2022; Hilton et al., 2002) as well as for assessing the influence of recycled subducting slab phases
67 (Fischer et al., 2002; Halldórsson et al., 2013; Mitchell et al., 2010; Sano and Marty, 1995). On the scale
68 of individual volcanic systems, such information is valuable for understanding magmatic volatile
69 budgets and for interpreting the chemistry of gas emissions. Considering a group of volcanoes,
70 whether within the same arc or in different arcs, we can learn about the variable efficiency of volatile
71 recycling during subduction according to differences in the phases present on the slab and the
72 pressure-temperature path experienced by the slab as it sinks (Aiuppa et al., 2019; Hilton et al., 2002;
73 Plank and Manning, 2019). Taken globally, these insights into volatile recycling efficiency during
74 subduction contribute to our understanding of the secular evolution of mantle and atmospheric
75 composition, plate tectonics, environmental change, and planetary habitability (Bekaert et al., 2021;
76 Hilton et al., 2002; Jambon, 1994).

77 Our understanding of magmatic volatile budgets at Rabaul and of volatile recycling in the wider New
78 Britain subduction zone is at an early stage. In this study, we have characterised the isotopic and
79 chemical of fumaroles on the active cone Tavurvur and hot springs around Rabaul caldera for the first
80 time. Many of our samples are affected by air contamination, potentially due to shallow seawater
81 intrusion or air circulation in the hydrothermal system within the poorly consolidated rocks of the
82 volcanic edifice. Nonetheless, by combining a range of complementary chemical and isotopic tracers,
83 along with a compilation of the available geochemical and isotopic data from whole rock analyses, we
84 have determined the provenance of volatiles at Rabaul. We find a strong mantle influence, based on
85 high ³He/⁴He values, and evidence from δ¹³C and δ¹⁵N for slab-derived carbonate and organic
86 sediment contributions.



87
 88 **Figure 1. A.** Map of New Britain, highlighting tectonic or geographic features mentioned in the text
 89 and selected volcanoes of the West Bismarck, New Britain, and Tabar-Lihir-Tanga-Feni groups. Of the
 90 volcanoes shown, all except Tabar, Tanga and Narage have reported Holocene activity (Global
 91 Volcanism Program, 2013). Map modified from (Holm et al., 2016; Macpherson et al., 1998). Inset
 92 shows location of PNG within Oceania. **B.** Google Earth image showing Rabaul caldera with major
 93 features (urban areas, volcanic edifices, our sampling sites) highlighted.

94 2. Geological Context

95 2.1 Tectonic Setting

96 Rabaul is located on the Gazelle Peninsula of New Britain in a complex tectonic setting between the
 97 converging Pacific and Australian plates (Holm et al., 2016; Woodhead et al., 1998). The island is built
 98 of Eocene-Oligocene volcanic rocks and intrusives, with overlying Miocene limestones and younger
 99 volcanics. Modern convergence is accommodated by microplate rotation and subduction of the
 100 Solomon Sea beneath the Bismarck Sea (Figure 1). The convergence rate at the New Britain trench is
 101 $\sim 9\text{-}13\text{ cm yr}^{-1}$ (Holm et al., 2016; Tregoning et al., 2000, 1998). New Britain's Paleogene volcanic and
 102 igneous rocks are related to an earlier period of subduction, when the Pacific plate was subducted
 103 along the now inactive Vitiaz-West Melanesian trench to the northeast of modern New Ireland (Figure
 104 1). Subduction along this margin ended around 26-20 Ma, possibly caused by the docking of the
 105 Ontong-Java plateau with the trench. The pause between these two phases of arc magmatism
 106 permitted the development of platform carbonates, in the Gazelle Peninsula represented by the Yalam
 107 Formation (Lindley, 2006; Madsen and Lindley, 1994).

108 The Solomon Sea slab dips $\sim 70^\circ$ northwards beneath the Gazelle Peninsula, steepening to subvertical
 109 towards its western end at 149° E (Zhang et al., 2023). Rabaul is $\sim 148\text{ km}$ above the slab (Syracuse and
 110 Abers, 2006). The subducting crust age is 24-44 Ma based on heat flow measurements (Joshima and
 111 Honza, 1986) and 28-34 Ma based on magnetic lineations (Joshima et al., 1986). There are no ocean
 112 drill cores of the Solomon Sea but samples of seafloor sediments and basalts obtained by dredges and
 113 freefall grabs from the R.V. *Natsushima* in 1983-4 may represent the subducting slab lithologies. The
 114 sediments are hemipelagic lower bathyal deposits comprising claystones and tuffaceous calcareous
 115 muds (Crook, 1986). The volcanic samples are variably altered ferrobasalts, both quench-textured
 116 lavas and devitrified hyaloclastites (Davies and Price, 1986). The major and trace element chemistry
 117 and Sr-Nd-Pb isotopic composition of these rocks was reported by Woodhead et al. (1998). Sediments
 118 sampled from the upper New Britain trench wall comprise a complex suite of limestones, glauconite-
 119 bearing sediments, and arenites and rudites derived from both volcanic rocks and carbonates (Crook,
 120 1986). At the western end of the trench, there is a 2.5 km-thick accretionary prism which is absent at
 121 the eastern end, closest to Rabaul (Honza et al., 1989). It remains unclear whether the uneven
 122 distribution of sediment in the New Britain trench is a consequence of lateral sediment transport
 123 caused by oblique plate convergence, greater debris infill at the western end due to proximity to the
 124 Western Bismarck arc and Australian continent collision zone, efficient subduction of sediment at the
 125 eastern end of the trench, or an eastward increase in tectonic erosion of the forearc crust (Bernstein-
 126 Taylor et al., 1992; Galewsky and Silver, 1997; Honza et al., 1989; Malatesta et al., 2013).

127 2.2 Eruptive History of Rabaul

128 Volcanism on the Gazelle Peninsula dates from the Lower to Middle Pleistocene and is distributed
 129 across four major centres, the Varzin Depression, the Vanakunau Basin, the submarine Tavui caldera
 130 and Rabaul, the most active (Hohl et al., 2022; Nairn et al., 1995). The oldest dated deposits at Rabaul
 131 ($\sim 0.5\text{ Ma}$) are associated with three basaltic stratovolcanoes, Tovanumbatir, Kombiu and Turangunan,
 132 adjacent to the modern caldera. Since 0.125 Ma, nine ignimbrite-forming eruptions have occurred,
 133 most recently the Rabaul Pyroclastics event in 667-699 CE, which deposited an 11 km^3 ignimbrite and
 134 formed a $6\times 8\text{ km}$ caldera (McKee et al., 2015; Nairn et al., 1995). Historical eruptions have occurred
 135 at multiple vents within the caldera (Tavurvur, Vulcan, Rabalanakaia, Sulfur Creek, Palangiagia),
 136 including events (1878, 1937, 1994) where Vulcan and Tavurvur erupted simultaneously. The post-
 137 caldera eruptions exhibit lava flows, violent Strombolian behaviour, and Vulcanian to sub-Plinian
 138 blasts, with the diversity in eruption dynamics attributed to variations in magma ascent rate (Bernard
 139 and Bouvet de Maisonneuve, 2020). Caldera-forming eruptions are of dacitic composition while post-

140 caldera eruption products range from basaltic andesite to trachydacite (58-64 wt% SiO₂) (Bernard and
141 Bouvet de Maisonneuve, 2020; Fabbro et al., 2020; Nairn et al., 1995). Intermediate magmas at Rabaul
142 apparently result from the mingling and mixing of recharging basalts and resident dacites (Bouvet de
143 Maisonneuve et al., 2015; Patia et al., 2017). There has been no eruption at Rabaul since August 2014.

144 **2.3 Previous Work on Magma and Volatile Sources**

145 The mantle wedge beneath New Britain, of Indian MORB affinity based on whole-rock Pb isotopes, is
146 exceptionally depleted in high field strength elements (HFSE), a consequence of prior melting in the
147 back arc, i.e. Manus Basin (Woodhead et al., 1998). Post-Miocene New Britain volcanics are enriched
148 in fluid mobile elements (e.g. Ba/La, Sr/Nd), resulting from slab fluids infiltrating the mantle wedge
149 (DePaolo and Johnson, 1979; Johnson, 1979). Based on Sr-Nd-Pb isotopes, high Sr/Nd and low Th/Yb,
150 Woodhead et al. (1998) described New Britain volcanics as an end-member suite among global arcs,
151 bearing a strong influence of hydrous fluids derived from altered basaltic crust with relatively minor
152 influence of recycled sediments. This interpretation was previously advanced on the basis of lava B/Be
153 ratios (Morris et al., 1990). New Britain arc volcanoes lie over a remarkably wide range in depth to the
154 slab, from ~100 km at the volcanic front to ~600 km at the Witu Islands (Johnson, 1979; Woodhead
155 and Johnson, 1993). Tracers of slab fluid in the erupted lavas (e.g. Ba/La, Sr/Nd, ²⁰⁶Pb/²⁰⁴Pb, Eu
156 anomaly) diminish from south to north across the arc, suggesting a decrease in fluid influence with
157 increasing depth to slab. This trend is convolved with increasing HFSE concentration, reflecting a
158 decrease in partial melting, also correlated with depth to slab (DePaolo and Johnson, 1979; Woodhead
159 et al., 1998; Woodhead and Johnson, 1993). Rabaul is not included in the Woodhead et al. (1998)
160 study, though the authors note that limited Sr-Pb isotopic analyses of 1994 Vulcan and Tavurvur
161 andesites are notably more radiogenic than other New Britain rocks (Johnson et al., 1995) and that
162 this may be a consequence of 'paleo-enrichment' of the mantle wedge, related to the earlier
163 subduction of the Pacific plate (see section 2.1). More recent work (Hohl et al., 2022), argues for the
164 influence of both slab-derived fluids and slab sediment-derived melts on the mantle beneath Rabaul,
165 based on trace element and Sr-Nd-Hf isotope analyses of 'inner caldera' (post-1400 B.P. eruptions of
166 Tavurvur, Vulcan, Rabalanakaia, Sulphur Creek) and outer caldera (undated rocks from neighbouring
167 mafic stratovolcanoes, e.g. Kombiu) deposits.

168 Studies of gas emissions from Rabaul and other PNG volcanoes have largely focussed on determining
169 SO₂ and CO₂ flux, using drone-based sensing (Galle et al., 2021; Liu et al., 2020; McCormick Kilbride et
170 al., 2023), ground-based remote sensing (Andres and Kasgnoc, 1998; McGonigle et al., 2004) or
171 satellite observations (Carn et al., 2017; McCormick et al., 2012). These data show that PNG volcanoes
172 (specifically Rabaul, Manam and Bagana) are globally important sources of both SO₂ and CO₂ (Aiuppa
173 et al., 2019; Carn et al., 2017; Fischer et al., 2019). Analyses of gas chemistry are more restricted. Soil
174 CO₂ emissions at Rabaul were sporadically monitored in the 1990s (Global Volcanism Program, 1997a,
175 1997b, 1995). Otherwise, there are two measurements of helium isotopes in hot spring gases (Farley
176 et al., 1995) and two measurements of helium and carbon isotopes in gas samples from Tavurvur and
177 Rabalanakaia (Sano and Williams, 1996). The helium isotopes range from 5.7-8.6 R/R_A, indicating a
178 predominantly mantle-derived helium with little crustal input. The carbon isotopes (δ¹³C) range from
179 -2.55 to -2.80 ‰, consistent with mixing between carbonate and mantle-derived carbon. Recent
180 global compilations of arc outgassing have suggested that the high carbon fluxes from PNG volcanoes
181 are due to efficient recycling of subducted carbon, though no distinction is made between the
182 tectonically and geochemically distinct West Bismarck, New Britain and Bougainville arcs in these
183 studies (Aiuppa et al., 2019, 2017; Plank and Manning, 2019). In contrast, other work argued for
184 remobilized crustal carbonate as the main source of volcanic CO₂ in PNG (Mason et al., 2017). Here,
185 our aim is to discriminate between these scenarios, and moreover to determine the influence of
186 sediment recycling on Rabaul gas emissions.

187 **3. Methods**188 **3.1 Sampling Methods**

189 We sampled multiple sites of gas emissions at Rabaul across two field expeditions, in September 2016
190 and May 2019. In 2016, we collected gas samples from a fumarole at the base of Tavurvur crater, from
191 hot springs on the beach north of Tavurvur towards Sulfur Point, and from hot springs at Rababa
192 (Figure 1b). In 2019, we sampled fumaroles on the northeast rim of Tavurvur and re-sampled Rababa
193 hot springs (Figure 1b).

194 We collected fumarolic gases by inserting a titanium tube into the fumarole and connected this tube
195 to our sampling line, composed of a Giggenbach bottle and multiple copper tubes connected in series
196 using silicon tubing. The 2019 Giggenbach bottle was an evacuated glass flask containing 5M NaOH
197 solution (Broadley et al., 2020; Giggenbach, 1975; Giggenbach and Goguel, 1989). In 2016, the
198 Giggenbach bottle was evacuated, but did not contain any NaOH solution.

199 We collected hot spring samples by placing an inverted plastic funnel over a persistent bubbling area,
200 securely immersing the funnel in the hot spring pool, and connecting it to the Giggenbach bottle and
201 copper tubes with silicon tubing (Barry et al., 2022). At all sites, we allowed the line to be flushed with
202 gas for at least 30 minutes prior to collecting our samples. At the fumarole site and the bubbling
203 springs we also collected gas samples into Tedlar bags for carbon isotopic analyses.

204 We sampled gases from the Tavurvur crater floor fumaroles in 2019 by means of an uncrewed aerial
205 system (UAS), comprised of a multi-rotor DJI Phantom airframe equipped with a Tedlar gas bag
206 sampling apparatus (Galle et al., 2021; Liu et al., 2020). We determined that the aircraft was in the
207 plume by visual observations and triggered sample capture by means of a set timer.

208

209 **3.2 Analytical Methods**

210 Our samples have been analysed in multiple laboratories in several institutions: the University of
211 Oxford (UO), the University of Manchester (UM, both UK), Woods Hole Oceanographic Institution
212 (WHOI) and the University of New Mexico (UNM, both USA).

213 *Gas chemistry.* We analysed headspace gases from the Giggenbach bottles using a combination of gas
214 chromatography and quadrupole mass spectrometry. Dissolved gases from the Giggenbach bottles
215 were analysed using wet chemical techniques and ion chromatography. The analytical procedures
216 have been recently described (Ilanko et al., 2019; Lee et al., 2017). In short, the gas chromatograph
217 with a Discharge Ionization Detector and helium carrier gas was used to determine N₂, Ar+O₂, CO₂, CO,
218 CH₄ and H₂ and the quadrupole was used to quantify Ar, O₂, He, and N₂. The NaOH solution was
219 analysed for CO₂ by alkalinity titration. Sulfur species were analysed by ion chromatography and
220 alkaline iodine titration. Chlorine and fluorine were analysed by ion chromatography.

221 *Helium isotopes.* Our noble gas analyses followed similar procedures between labs, whether at UO,
222 UM or WHOI (Barry et al., 2022, 2016). At UO, the instruments were an SFT and an ARGUS, at UM a
223 modified VG5400 with upgraded electronics, and at WHOI a Nu Noblesse. We connected copper tubes
224 to the respective extraction lines using an O-ring connection, and released small volumes (2-20 cm³)
225 of gas sample into the sample clean-up lines. We removed reactive gases using a chemical procedure,
226 exposing the sample to a heated titanium sponge, and then passed the gases through (hot and cold)
227 getters. We then passed a small aliquot of cleaned gas into a cryogenic trap, which allowed separation
228 of each noble gas. The noble gases measured varied between labs. At UO, we measured all stable
229 noble gas isotopes, whereas at WHOI, we only measured He isotopes and ⁴He/²⁰Ne. We were unable

230 to measure Ne isotopes at UM, hence the lack of $^4\text{He}/^{20}\text{Ne}$ data for these samples. Given the $^{40}\text{Ar}/^{36}\text{Ar}$
231 is very close to air, we could assume an air $^{20}\text{Ne}/^{22}\text{Ne}$ and $^4\text{He}/^{20}\text{Ne}$ for most samples. We estimate
232 uncertainties of $\leq 5\%$ for helium isotopes and $\leq 3\%$ for neon and argon isotopes.

233 *Carbon isotopes.* We analysed the Tedlar bag samples using a Delta-Ray Infrared Isotope analyser
234 (Fischer and Lopez, 2016; Galle et al., 2021; Liu et al., 2020). We set up the Delta Ray instrument at
235 Rabaul Hotel, in Rabaul Town (Figure 1b). The CO_2 -free air carrier gas was produced on-site by passing
236 air, pressurized in a tank, through Sulfolime absorbent. The calibration gas was pure CO_2 obtained
237 from a company in PNG. We did not know the $\delta^{13}\text{C}$ value of the calibration gas at the time of our
238 analyses in Rabaul, so we collected a sample of this gas and analysed it on the Delta Ray at the
239 University of New Mexico after our return and then retroactively corrected the values obtained during
240 the fieldwork.

241 *Nitrogen isotopes.* We performed nitrogen isotope measurements on gas splits from copper tubes. In
242 brief, our fumarole and hot spring gas samples were purified on a specially designed N gas extraction
243 vacuum line (Barry et al., 2012) and analysed for nitrogen isotopes on the Nu Noblesse at WHOI
244 (Bekaert et al., 2023). We placed a third stainless steel clamp on each tube approximately one-half
245 inch from one of the original clamps to subsample an aliquot of the gas in each tube. We connected
246 copper tubes to the extraction line with VCR fittings and pumped down to $<1 \times 10^{-7}$ Torr. Once
247 sufficient vacuum was achieved, we removed the exterior clamp to inlet the aliquot of gas. We froze
248 out condensable gases (mainly CO_2 and H_2O) on a cold finger using liquid nitrogen. The non-
249 condensable gases were expanded into the extraction line and diluted until the sample pressure was
250 low enough to be measured. We then exposed the gas to a Pt furnace at 1000°C and a CuO furnace
251 that was heated from 450°C to 850°C , held for 15 minutes to convert CO to CO_2 , and step cooled back
252 to 450°C over 30 minutes. A second cold finger with liquid nitrogen was used to freeze down the CO_2 .
253 Once the CuO furnace had cooled to its initial temperatures and CO conversion was complete, we
254 passed an aliquot of the gas into the mass spectrometer for analysis and typically performed each
255 analysis in triplicate. We ran line blanks prior to the analysis to use for correction and an air standard
256 following the analysis; the size of the standard is calibrated to match the size of the sample. We
257 applied a linearity correction to the samples using the line blanks and air standards (Bekaert et al.,
258 2023).

259

260

261

262 4. Results

263 The gas compositions (Figure 2) of our fumarole and hot spring gas samples are reported in Table 1.
264 The helium (Figure 3) and carbon (Figure 4) isotopic composition and relative abundance ratios (Figure
265 5) are reported in Table 2, along with our estimates of mantle- and slab-derived influences (after Sano
266 & Marty, 1995). In Table 3, we report the nitrogen isotopic composition (Figure 6) of our samples and
267 independent estimates of mantle- and slab-derived influences (after Sano et al., 2001).

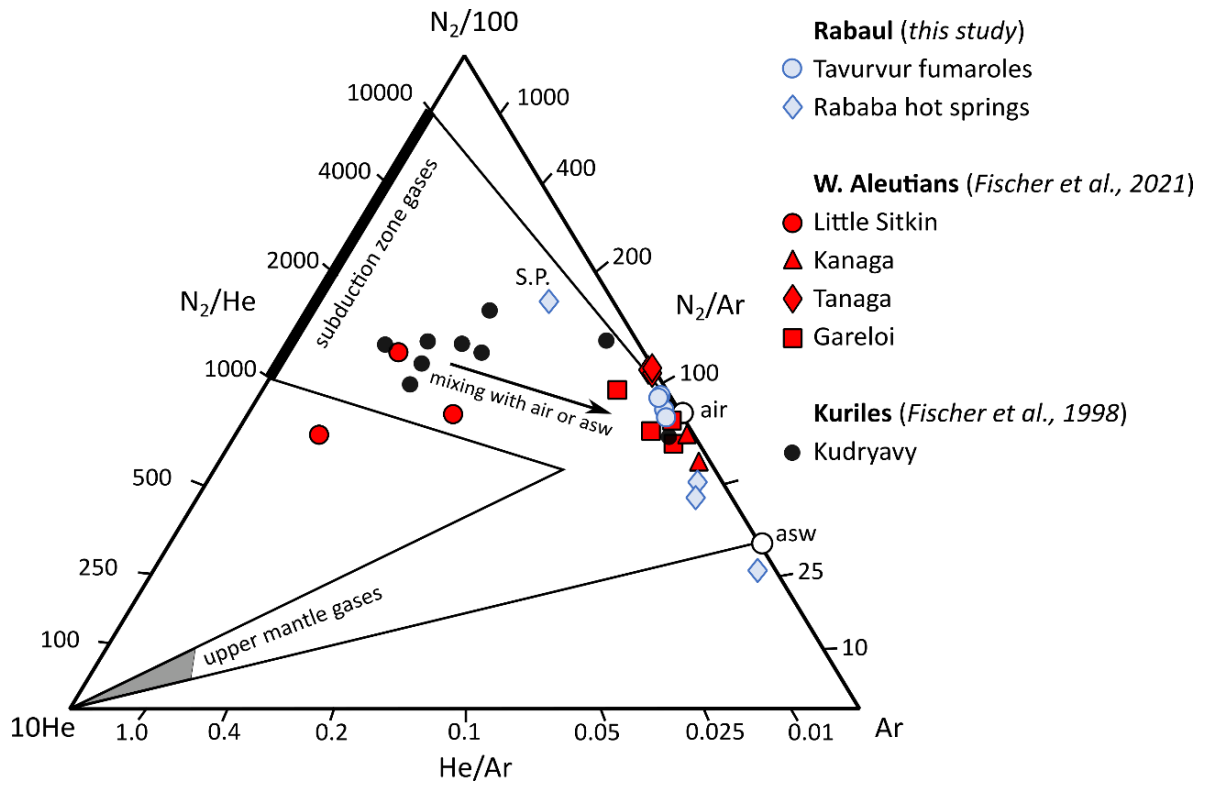
268

269 4.1 Gas chemistry

270 The abundance of major and minor gas species in Rabaul samples are reported in Table 1, with relative
271 N₂, He and Ar abundance shown in Figure 2. Samples from the 2016 field expedition were collected
272 without NaOH solution in the Giggenbach bottles, so we could not measure H₂O, sulfur or halogen
273 species in these gases. Samples collected in 2019 were dominated by H₂O (678 to 967 mmol/mol in
274 Tavurvur fumaroles, 773 mmol/mol in Rababa hot spring gases) with minor CO₂ (13 to 18 mmol/mol
275 in fumaroles and 222 mmol/mol in hot spring gases), and total S (S_t) (0.33 to 2.1 mmol/mol SO₂ and
276 0.33 to 2.10 mmol/mol H₂S in fumaroles, 0.06 mmol/mol SO₂ and 1.06 mmol/mol H₂S in hot spring
277 gases). CO₂/S_t in the fumarole gases collected in 2019 range from 5.7 to 6.1, slightly higher than what
278 was measured by a 2016 measurement by MultiGAS in Tavurvur's crater (2.6 - 2.8, Galle et al., 2021).

279 These gas compositions exhibit the high N₂/He ratios characteristic of volcanic arc gases worldwide,
280 and a wide range in He/Ar and N₂/Ar because of variable mixing between magmatic gases and air or
281 air-saturated water (ASW), in common with low-temperature arc emissions elsewhere (e.g., Fischer
282 et al., 2021). Air and ASW have N₂/Ar of 83 and 40 respectively (Fischer et al., 1998). The influence of
283 ASW is also consistent with the higher CO₂/S_t ratios measured in our Giggenbach bottle samples
284 compared to ratios based on MultiGAS measurements made on the crater floor (Galle et al., 2021).
285 Our samples exhibit high degrees of air or ASW contamination, evidenced by N₂/Ar < 100 and He/Ar <
286 0.01. Arc gases of pristine magmatic composition (e.g., Fischer et al., 1998) tend to have N₂/Ar >100,
287 higher He/Ar, and lower N₂/He; both N₂ and Ar excesses in volcanic gases can be attributed to air
288 contamination during sampling (Giggenbach, 1980).

289



290

291 **Figure 2.** Ternary diagram showing relative molecular nitrogen, helium and argon (N_2 -He-Ar)
 292 compositions of fumarole and hot spring gas samples from this study, to highlight magmatic versus air
 293 and ASW contributions (Giggenbach, 1980). Also shown are gas data from two other Pacific rim
 294 subduction zones (Fischer et al., 2021, 1998).

295

Site	Sample ID	T (°C)	H ₂ O	CO ₂	St	SO ₂	H ₂ S	HCl	HF	He	H ₂	Ar	O ₂	N ₂	CH ₄	CO	N ₂ /Ar	N ₂ /He	He/Ar
2019																			
Tavurvur rim fumarole	RB-19-1b	97	967	18.3	3.02	1.99	1.02	0.13	nd	0.00020	0.217	0.181	0.001	11.3	0.00070	nd	62	55780	0.001
Tavurvur rim fumarole	RB-19-6a	98	678	13.8	2.43	2.1	0.33	0.06	nd	0.00007	0.165	0.085	<0.001	5.35	0.00051	nd	63	77835	0.001
Rababa hot spring	RB-19-3a	75	773	222.0	1.13	0.06	1.06	0.43	0.07	0.00037	0.001	0.129	0.029	3.57	0.02741	nd	28	9596	0.003
2016																			
Tavurvur floor fumarole	Tav-2B	100		0.33						0.0014	nd	0.850	19.2	79.6	nd	nd	94	56872	0.002
Tavurvur floor fumarole	Tav-2A	140		0.45						0.0018	0.017	0.868	19.97	78.7	nd	nd	91	43720	0.002
Rababa hot spring	RB-HS-1	78		86.6						0.0011	nd	0.219	0.41	12.3	0.521	nd	56	11155	0.005
Rababa hot spring	RB-HS-3	78		72.9						0.0035	nd	0.497	1.03	25.4	0.083	nd	51	7267	0.007
Hot spring near Sulfur Pt.	RB-HS-2	82		71.60						0.0034	nd	0.128	1.07	27.2	0.046	nd	213	7986	0.026
MORB																	152 ± 58	48 ± 6	2
ASW																	40	150,000	0.0005

296

297

298

299

Table 1. Gas chemistry from fumarole and hot spring gases sampled at Rabaul. Data from 2019 campaign are reported as mmol/mol since we sampled with caustic solution in Giggenbach bottle and could isolate H₂O. Data from 2016 are reported as molar percent dry gas. Concentrations cannot be directly compared across these two campaigns, though N₂/Ar, N₂/He and He/Ar ratios can be. 'nd' signifies not detected.

300

301

Site	Sample ID	Lab	T (°C)	R/R _A	R _C /R _A	⁴ He/ ²⁰ Ne	X-value	⁴⁰ Ar/ ³⁶ Ar	⁸⁴ Kr/ ³⁶ Ar (×10 ⁻²)	¹³² Xe/ ³⁶ Ar (×10 ⁻²)	δ ¹³ C	CO ₂ / ³ He	% mantle He	% M	% L	% S
2019																
Tavurvur rim fumarole	RB-19-1b [‡]	WHOI	97	1.9	5.7	0.40	1.3	na	na	Na	-5.39	1.14 × 10 ¹⁰	71	17.5	67.4	15.0
Tavurvur rim fumarole	RB-19-1b_dup [‡]	WHOI	97	2.2	6.5	0.41	1.3	na	na	Na	na		81			
Tavurvur rim fumarole	RB-19-1b	UM	97	2.1		n.a.		300.7	3.83	2.02	na					
Tavurvur rim fumarole	RB-19-1b_dup	UM	97	2.3		n.a.		299.4	2.29	1.15	na					
Tavurvur rim fumarole	RB-19-1b2	UM	98	0.9		n.a.		298.9	2.00	1.00	na					
Tavurvur rim fumarole	RB-19-6a [‡]	WHOI	98	2.7	6.0	0.48	1.5	na	na	na	-4.61	2.39 × 10 ¹⁰	75	8.4	77.7	14.0
Rababa hot spring	RB-19-3a [‡]	WHOI	75	5.8	6.3	3.23	10.1	na	na	na	-3.67	6.71 × 10 ¹⁰	79	3.0	85.3	11.7
Rababa hot spring	RB-19-3a_dup [‡]	WHOI	75	6.1	6.7	2.78	8.7	na	na	na	-3.67		84			
Rababa hot spring	RB-19-3a1	UM	75	5.6		na		306.3	5.36	3.06	na					
Rababa hot spring	RB-19-3a2	UM	75	6.5		na		303.7	4.84	4.63	na					
Rababa hot spring	RB-19-3a2_dup	UM	75	6.5		na		303.9	5.69	3.48	na					
2016																
Tavurvur floor fumarole	Tav-2A	UO	140	1.0	n.d.	0.31	1.0	309.7	1.99	0.72	na	2.27 × 10 ⁸	9			
Rababa hot spring	RB-HS-1	UO	78	6.4	6.9	3.16	9.9	320.1	4.42	3.37	-4.5	8.04 × 10 ⁹	87	24.9	64.3	10.9
Hot spring near Sulfur Pt.	RB-HS-2	UO	82	3.3	6.2	0.46	1.5	318.6	1.68	2.31	-9.2	2.47 × 10 ⁹	77	81.1	1.8	17.2
Garbuna crater fumarole	Gar-F-343	UO	97	7.5	7.5	36.01	113.0	307.6	3.12	2.6	na		94			
Garbuna crater fumarole	Gar-F-344	UO	89	7.1	7.2	30.71	796.4	310.0	3.82	3.53	na		90			
Silanga village hot spring	Sil-HS-345	UO	76	5.3	5.4	20.03	62.9	314.3	3.51	2.35	na		67			
Pangalu hot spring	Pan-HS-1A	UO	87	6.3	6.6	5.41	17.0	313.5	na	na	na	6.75 × 10 ⁸	82			
Pangalu hot spring	Pan-HS-2	UO	100	2.3	6.7	3.51	11.0	312.3	3.18	2.03	-9.6	1.79 × 10 ⁹	84			

302

303

304

305

306

307

308

309

Table 2. Helium and carbon isotopes, relative abundance ratios, and estimates of mantle helium (Barry et al., 2013) and mantle (%M) and slab (limestone, %L, or sedimentary, %S) carbon (Sano and Marty, 1995) contributions from fumarole and hot spring gases sampled at Rabaul. Different noble gas isotope ratios were measured between laboratories and not all samples were analysed for δ¹³C ('na' signifies not analysed). [‡]Samples were splits from Giggenbach bottles, all others were copper tubes. Suffix "_dup" indicates duplicate analyses of the same copper tube or Giggenbach bottle split.

310 4.2 Helium isotopes

311 We have determined the helium isotope composition of 14 fumarole and hot spring gas samples from
 312 Rabaul (Figure 3, Table 2), reported as R/R_A values ($R = {}^3\text{He}/{}^4\text{He}$ in sample, $R_A = \text{atmospheric } {}^3\text{He}/{}^4\text{He}$
 313 $= 1.39 \times 10^{-6}$). Fumarole gases collected from Tavurvur's crater floor and rim range from 0.92 to 2.70
 314 R_A , while hot spring gases collected from Rababa range from 5.62 to 6.47 R_A , and hot spring gases
 315 collected near to Sulfur Point were 3.3 R_A . Figure 3 also shows helium isotope measurements from
 316 volcanic and geothermal gases we sampled elsewhere in New Britain during a reconnaissance survey
 317 in 2016: from fumaroles at the summit of Garbuna volcano, hot springs near Silanga village close to
 318 the Sulu Range, and hot springs from Pangalu village close to the Garua Harbour/Talasea volcanic field.
 319 We also plot helium isotope data from hot springs in Rabaul caldera, fumaroles from the Witu Islands,
 320 and various geothermal and fumarolic gases sampled across the nearby Tabar-Lihir-Tanga-Feni group
 321 (Craig and Poreda, 1987; Farley et al., 1995). Our helium isotope data from Rabaul hot springs overlap
 322 with those of Farley et al. (1995) and Sano & Williams (1996), excepting the Tavurvur sample from the
 323 latter study which has R/R_A of 8.6. Our samples from elsewhere in New Britain (Sulu, Garua Harbour,
 324 Garbuna) record slightly higher He isotope values with respect to Rabaul. Many of the TLF gases and
 325 the Witu Islands gases approach the MORB range, i.e. $\sim 8 \pm 1 R_A$ (Hilton et al., 2002).

326 For seven of our samples (Table 2), we use the ${}^4\text{He}/{}^{20}\text{Ne}$ value to apply an atmospheric correction,
 327 assuming that ${}^{20}\text{Ne}$ is derived from air (${}^4\text{He}/{}^{20}\text{Ne} = 0.32$) or air saturated water (ASW, ${}^4\text{He}/{}^{20}\text{Ne} = 0.26$
 328 at 15 °C) (Hilton, 1996; Ozima and Podosek, 2002). This allows us to calculate an atmospheric He value
 329 and subtract it from our measured ${}^3\text{He}/{}^4\text{He}$. Our sample collected on the floor of Tavurvur crater has
 330 ${}^4\text{He}/{}^{20}\text{Ne}$ very close to ASW, suggesting substantial atmospheric contamination, while our remaining
 331 samples (Sulfur Point and Rababa hot springs at Rabaul, plus our samples from elsewhere in New
 332 Britain) have significantly higher ${}^4\text{He}/{}^{20}\text{Ne}$ suggesting lesser atmospheric contributions (Figure 3b). Our
 333 correction is based on the methods of (Hilton, 1996), using 'X-values' to correct helium isotope ratios
 334 for atmospheric influence. The X-value of a gas sample is defined as:

$$335 (X)_{\text{gas}} = ({}^4\text{He}/{}^{20}\text{Ne})_{\text{measured}} / ({}^4\text{He}/{}^{20}\text{Ne})_{\text{air}}$$

336 where $({}^4\text{He}/{}^{20}\text{Ne})_{\text{measured}}$ is the measured ratio and $({}^4\text{He}/{}^{20}\text{Ne})_{\text{air}}$ is the value of air, 0.32.

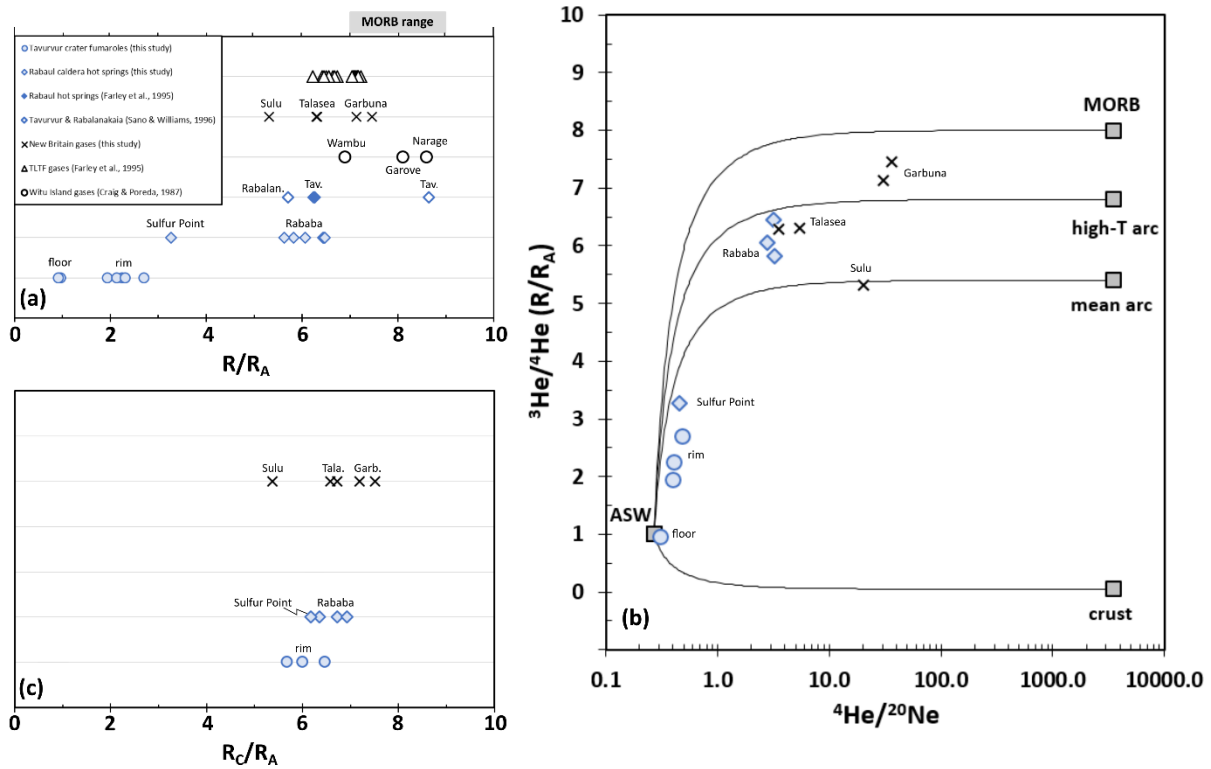
337 We can then combine our X-values with measured helium isotope values (R/R_A) to calculate
 338 atmospheric corrected values (R_C/R_A):

$$339 R_C/R_A = ((R/R_A \times X) - 1) / (X - 1)$$

340 where R_C/R_A is reported relative to air ($= 1.39 \times 10^{-6}$). Our samples from Tavurvur rim fumaroles and
 341 Rababa and Sulfur Point hot springs show air-corrected He isotope (R_C/R_A) values ranging from 5.7 to
 342 6.9 (Table 2, Figure 3c). Tavurvur samples show greater air contamination than the hot spring samples.
 343 We consider the least air contaminated sample of Rababa hot spring, R_C/R_A of 6.7, as the most
 344 representative value of the Rabaul magmatic system. These helium isotope values are below the
 345 canonical range for upper mantle helium ($8 \pm 1 R_A$) and high above the range associated with
 346 radiogenic (i.e., crustal) helium, 0.05 R_A (Andrews, 1985), suggesting that all samples are a mixture of
 347 mantle and radiogenic sources. With regards to helium isotope values in volcanic arcs globally, our
 348 samples are consistent with the average high temperature fumaroles in volcanic arcs globally of 6.8
 349 R_A (Kagoshima et al., 2015) and within the overall average range of gases emitted from fumaroles and
 350 hot springs of arc volcanoes of $5.4 \pm 1.9 R_A$ (Hilton et al., 2002) (Figure 3c).

351 We measured the isotopic composition of heavy noble gases in a subset of our samples, shown in
 352 Supplementary Figure 1. Most cluster around the composition of air and air-saturated water, though
 353 there is evidence for higher ${}^{84}\text{Kr}/{}^{36}\text{Ar}$ and ${}^{132}\text{Xe}/{}^{36}\text{Ar}$ in all samples from Rababa hot springs.

354



355

356 **Figure 3.** (a) Helium isotopes measured in fumarole and hot spring gases from Rabaul (this study,
 357 Farley et al., 1995; Sano & Williams, 1996), and other volcanoes on New Britain and neighbouring
 358 islands (Craig and Poreda, 1987; Farley et al., 1995); (b) the same data plotted versus ${}^4\text{He}/{}^{20}\text{Ne}$ along
 359 with calculated binary mixing lines between air saturated water (ASW) and crustal and mantle
 360 endmember compositions (Barry et al., 2021; Hilton et al., 2002; Kagoshima et al., 2015); (c) air-
 361 corrected helium isotopes for our new Rabaul and New Britain samples.

362

363 **4.3 Carbon isotopes**

364 Gases emitted from a vent in the floor of Tavurvur crater, and sampled by our UAS, range in CO₂
365 concentration from 432 to 555 ppm, with $\delta^{13}\text{C}$ varying from -6.48 ± 0.17 to -8.95 ± 0.03 ‰, with respect
366 to the Pee Dee Belemnite (PDB) reference standard (Table 3, Figure 4). We measured higher CO₂
367 concentrations and more positive carbon isotope compositions in fumarole gases collected on the
368 crater rim (709 to 949 ppm CO₂, -4.61 ± 0.55 to -5.39 ± 0.07 ‰ $\delta^{13}\text{C}$) and in Rababa hot spring gases
369 (2506 to 2646 ppm CO₂, -3.67 ± 0.06 ‰ $\delta^{13}\text{C}$). Over the course of our one-week campaign, there was
370 no significant temporal variation in $\delta^{13}\text{C}$ at each site. Clean air collected on a beach away from volcanic
371 plume influence had a CO₂ concentration of 430 ppm and $\delta^{13}\text{C}$ of -7.70 ± 0.05 . On a Keeling plot
372 (Keeling, 1958), our data fall along a linear regression and the extrapolated $\delta^{13}\text{C}$ value of the pure
373 source CO₂ is estimated to be -2.6 ± 0.62 ‰ (Figure 4).

374

375 **4.4 CO₂/³He values**

376 Our samples span a range in CO₂/³He over an order of magnitude from $\sim 2.5 \times 10^9$ to 6.7×10^{10} (Figure
377 5). The minimum value is in the hot spring gases collected near Sulfur Point and lies within the MORB
378 range of CO₂/³He, $1\text{--}6 \times 10^9$ (Marty et al., 2020). Our samples from both Rababa hot springs and the
379 Tavurvur crater rim fumarole are consistent with the addition of carbon from subducted or crustal
380 limestones. Our sample from Rababa collected in 2019 has higher CO₂/³He than the sample collected
381 in 2016, 6.7×10^{10} compared to 8.0×10^9 . All our samples lie in a region of CO₂/³He space bounded by
382 mixing curves between MORB, subducted organic sediment and marine limestone end-members,
383 suggesting that the carbon emitted in volcanic gases at Rabaul is partly supplied by all three of these
384 sources.

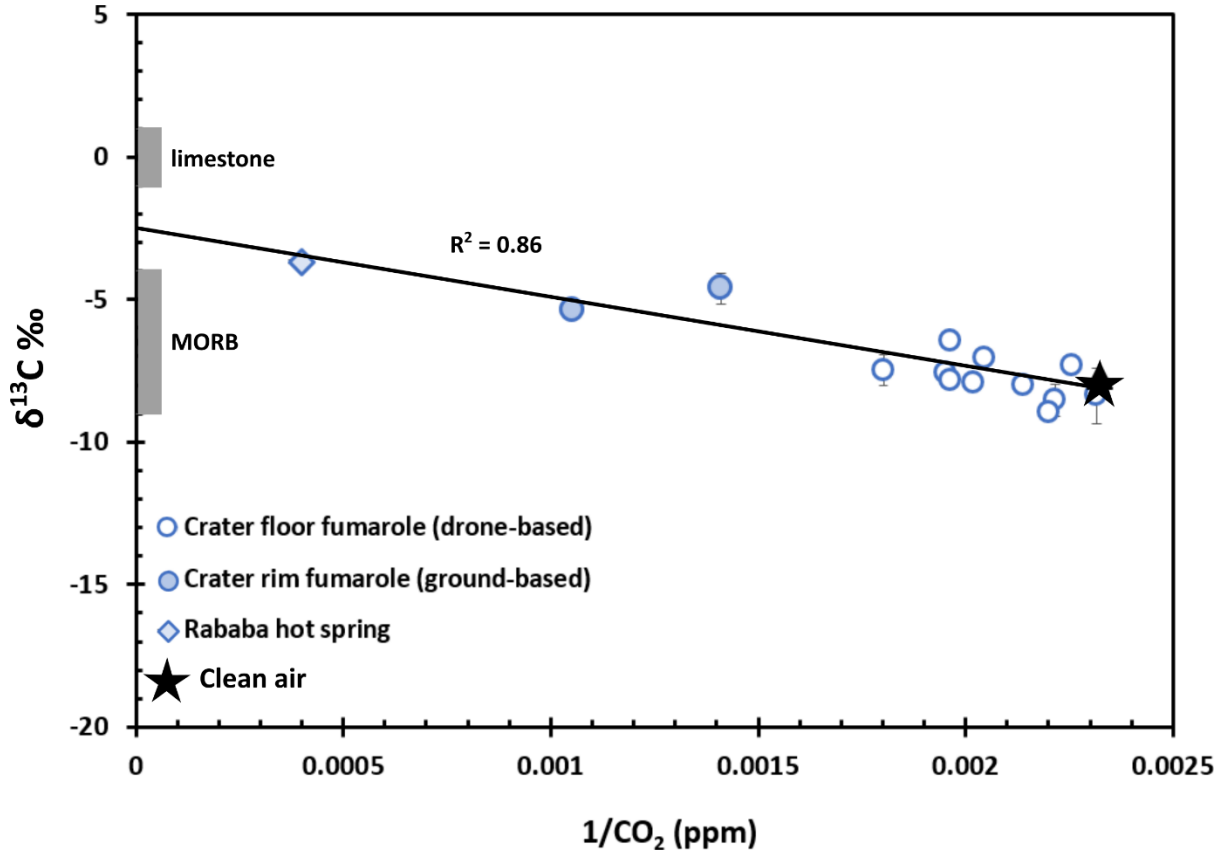
385

386 **4.5 Nitrogen isotopes**

387 We report nitrogen isotope data in delta notation, where $\delta^{15}\text{N}$ is the per mil (‰) deviation of the
388 measured ¹⁵N/¹⁴N from that of air, which has $\delta^{15}\text{N} = 0$ ‰. Measured $\delta^{15}\text{N}$ ($\pm 1\text{-}\sigma$ errors) range from -
389 0.75 ± 0.50 to 1.99 ± 0.80 ‰ in Tavurvur crater rim fumarole samples and from 0.16 ± 0.18 to $4.56 \pm$
390 0.63 ‰ in Rababa hot spring samples (Table 4, Figure 6). N₂/He ranged from 55780 to 77835 in
391 Tavurvur crater gases and from 9596 to 11155 in Rababa hot spring gases. Our samples from Tavurvur
392 crater are likely to be air contaminated (see Section 5.3). The positive enrichment in N isotopes
393 observed in the Rababa hot springs samples is comparable to that seen in volcanic gases in other
394 circum-Pacific arcs where nitrogen is supplied both from the mantle and from sediments carried on
395 the subducting slab (Clor et al., 2005; Fischer et al., 2005, 2002; Mitchell et al., 2010).

396

397



398

399

400 **Figure 4.** Relationship between carbon concentration and δ¹³C for fumarole and hot spring gases at
 401 Rabaul. The typical δ¹³C range for reference endmembers are also shown: limestone (subducted
 402 marine carbonate, δ¹³C ~0 ‰) and MORB (upper mantle material, δ¹³C ~-6.5 ± 2.5). The black line
 403 indicates a mixing line projected from ambient air through the composition of gases sampled from
 404 Taurvur crater floor and rim fumaroles and Rababa hot springs.

405

406

407

Sample ID	Date	Sampling Site	CO ₂ (ppm)	$\delta^{13}\text{C}$	+/-
TAV-CRF_1401	14/05/21	crater floor	467	-8.02	0.11
TAV-CRF_1402	14/05/21	crater floor	489	-7.06	0.07
TAV-CRF_1403	14/05/21	crater floor	432	-8.38	0.96
TAV-CRF_1404	14/05/21	crater floor	451	-8.54	0.58
TAV-CRF_1405	14/05/21	crater floor	443	-7.34	0.09
TAV-CRF_1601	16/05/21	crater floor	512	-7.60	0.16
TAV-CRF_1602	16/05/21	crater floor	509	-7.86	0.09
TAV-CRF_1603	16/05/21	crater floor	495	-7.94	0.06
TAV-CRF_1604	16/05/21	crater floor	454	-8.95	0.03
TAV-CRF_1605	16/05/21	crater floor	555	-7.48	0.54
TAV-CRF_1606	16/05/21	crater floor	509	-6.48	0.17
TAV-CRR_1601	16/05/21	crater rim	709	-4.61	0.55
TAV-CRR_1601	16/05/21	crater rim	949	-5.39	0.07
RAB-HS1_1701	17/05/21	Rababa hot spring	2646	-3.67	0.06
RAB-HS1_1702	17/05/21	Rababa hot spring	2506	-3.67	0.03
RAB-AIR_1701	17/05/21	clean air	430	-7.70	0.05

408

409

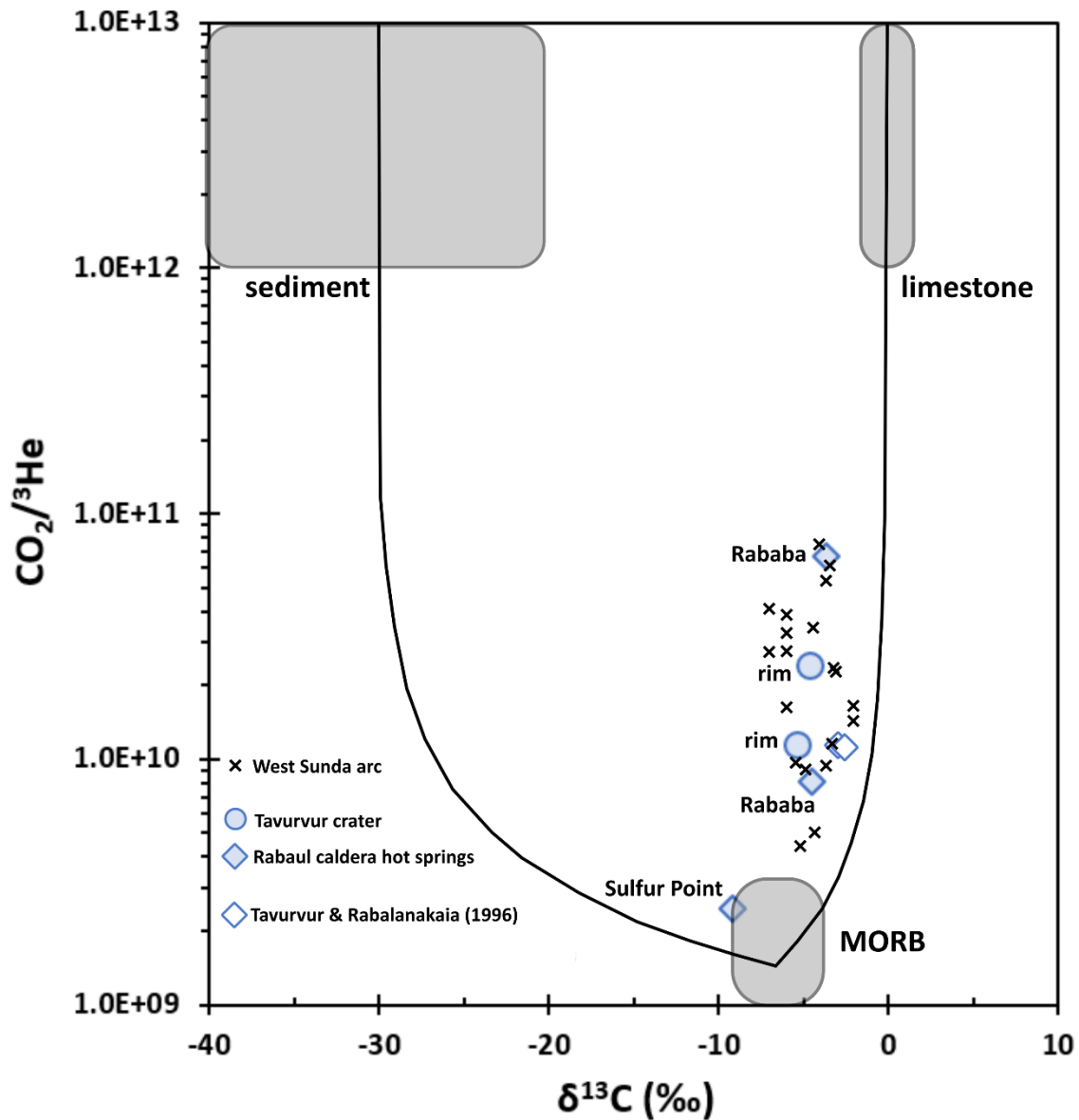
410

411

412

413

Table 3. Carbon isotopes and measured CO₂ concentration in fumarole and hot spring gases. Crater floor fumaroles and clean air were sampled using a Tedlar bag onboard our multicopter UAS and analysed by Delta Ray during the fieldwork. The remaining samples were collected using Giggenbach bottles and analysed by IRMS at UNM.

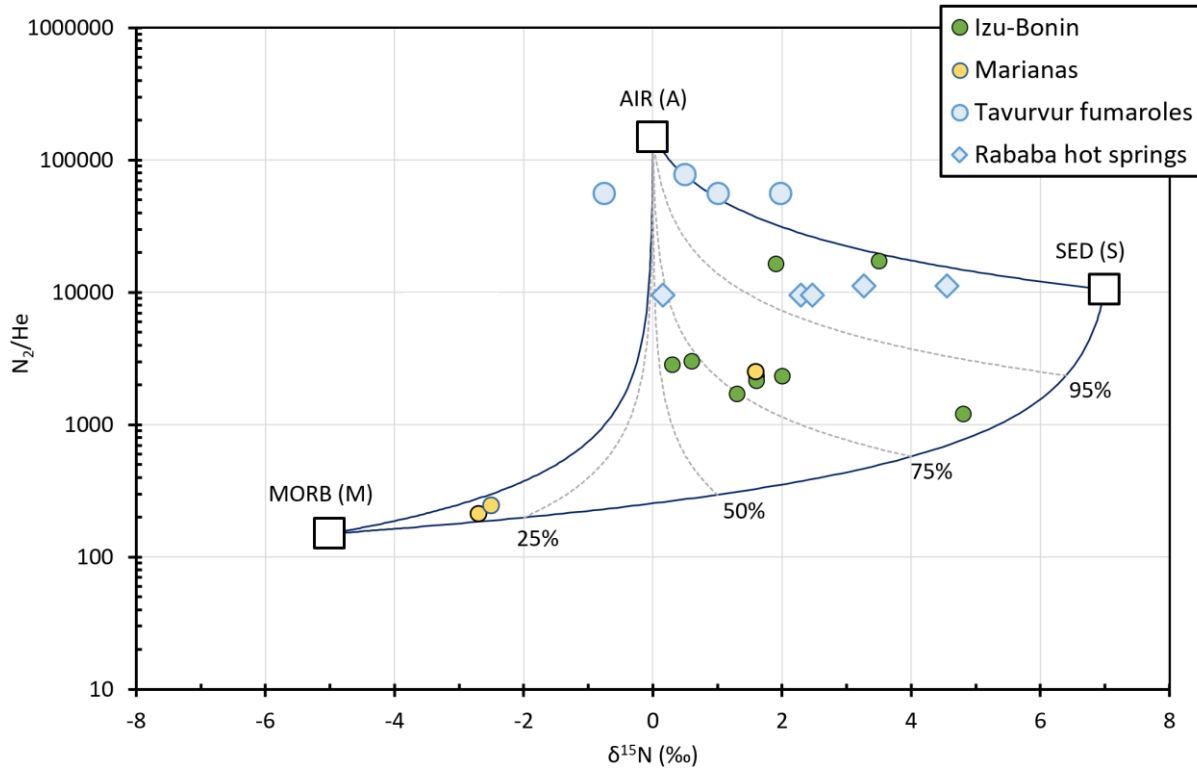


414

415 **Figure 5.** Three component mixing diagram between $CO_2/{}^3He$ and $\delta^{13}C$ (CO_2), after (Sano and Marty,
 416 1995). We show new data from Rabaul (Table 2), comprising caldera hot springs and Tavorvur crater
 417 fumaroles, previous measurements from Rabaul (Tavorvur and Rabalanakaia) made in 1996 (Sano and
 418 Williams, 1996) and published data from thirteen volcanic centres in Sumatra (Halldórsson et al.,
 419 2013). Model end-members of mid-ocean ridge basalt (MORB), marine limestone (including slab
 420 carbonate) and organic sediment are also shown, as grey boxes (Sano and Marty, 1995; Sano and
 421 Williams, 1996). Black lines show mixing among the end-members.

422

423



424

425 **Figure 6.** N_2/He vs. $\delta^{15}N$, with mixing lines between air, sediment and mantle end members. Labelled
 426 dashed lines represent mixing (% sediment) between mantle and sediment. We also show data from
 427 the Izu-Bonin and Northern Marianas arcs (Mitchell et al., 2010).

428

Site	Sample ID	Mean $\delta^{15}\text{N}$	N_2/He	% M	% A	% S	% M_c	% S_c	$\delta^{15}\text{N}_c$
2019									
Tavurvur rim fumarole	RB-19-1 A	1.02 ± 0.33	55780	0.3	85.0	14.7	1.8	98.2	6.79
Tavurvur rim fumarole	RB-19-1 C	1.99 ± 0.80	55780	0.3	71.1	28.6	0.9	99.1	6.89
Tavurvur rim fumarole	RB-19-1b C	-0.75 ± 0.50	55780	0.3	-10.6	110.3	-2.6	102.6	7.31
Tavurvur rim fumarole	RB-19-6a A	0.50 ± 0.53	77835	0.2	92.6	7.2	2.6	97.4	6.69
Rababa hot spring	RB-19-3a B	0.16 ± 0.18	9596	1.6	95.0	3.4	31.6	68.4	3.21
Rababa hot spring	RB-19-3a B_dup	2.29 ± 0.42	9596	1.6	64.5	33.9	4.4	95.6	6.47
Rababa hot spring	RB-19-3a C	2.47 ± 0.56	9596	1.6	62.1	36.3	4.1	95.9	6.51
2016									
Rababa hot spring	RAB HS 1 A	4.56 ± 0.63	11155	1.3	32.6	66.1	2.0	98.0	6.76
Rababa hot spring	RAB HS 1 B	3.27 ± 0.65	11155	1.3	51.1	47.6	2.8	97.2	6.67

429

430

431

432

433

Table 4. Nitrogen isotopes and estimated mantle (M), atmospheric (A) and sediment (A) percentage contributions from fumarole and hot spring gases sampled at Rabaul. M_c and S_c are percentage contributions of mantle versus sediment influence on air-corrected nitrogen isotope values, $\delta^{15}\text{N}_c$. Capital letter suffixes (A, B, C) in the sample ID column refer to separate copper tube splits of our Giggenbach bottle samples. Where present, 'dup' refers to a duplicate. Each line in the table represents the mean and standard deviation of a triplicate analysis of each copper tube split.

434 5. Discussion

435 5.1 Atmospheric contamination

436 Before determining volatile provenance at Rabaul, we must first evaluate sample integrity, specifically
 437 potential contamination by atmospheric components such as air or air-saturated water. Key indicators
 438 of substantial air contamination can include high N_2/He (43720-56872), low He/Ar (0.002) and high O_2
 439 (19.2-20.0 mol%), typified by our samples from Tavurvur crater floor (Table 1). Atmospheric
 440 contamination may be introduced during sample collection or, more likely, via abundant air-saturated
 441 steam circulating in the poorly consolidated Tavurvur cone. Tavurvur rim fumarole samples, are less
 442 air contaminated, i.e., have O_2 of < 0.002 . All our samples fall close to either air or air-saturated water
 443 ($N_2/Ar = 80$ and 43 respectively) in a N_2 - He - Ar ternary diagram (Figure 2), indicating that all are subject
 444 to variable degrees of atmospheric contamination. This is further suggested by a range in $^{40}Ar/^{36}Ar$ of
 445 298.9-320.1, only slightly above the atmospheric value of 295.6 ± 0.5 , (Lee et al., 2006). Rababa hot
 446 spring samples exhibit lower N_2/He (7267-9596) and higher $^{40}Ar/^{36}Ar$ (303.7-320.1) than Tavurvur
 447 crater floor or rim samples (Table 1).

448 Helium isotopes and $^4He/^{20}Ne$ (Table 2, Figure 3) allow us a further means of evaluating variable
 449 degrees of atmospheric contamination. Tavurvur samples, both crater floor and rim, have low He
 450 isotope values (0.9 - $2.7 R_A$) and $^4He/^{20}Ne$ (0.3 - 0.4), indicating a strong atmospheric influence.
 451 Conversely, Rababa hot spring samples have higher R/R_A (5.6 - 6.5) and $^4He/^{20}Ne$ (2.78 - 3.23), indicating
 452 less contamination. Helium isotopes can be corrected for air contamination using X -values as
 453 described in Section 4.3.

454 Overall, on the basis of gas chemistry and He - Ne - Ar isotopes, we judge our Tavurvur (and Sulphur
 455 Point) samples to be heavily overprinted by atmospheric influence. This atmospheric contamination
 456 significantly affects gas species that are abundant in air, i.e. primarily nitrogen and therefore makes
 457 the determination of nitrogen sources in Tavurvur and Sulphur Point gases challenging. Our Rababa
 458 hot spring gases indicate a mixture of magmatic and atmospheric influence and can be used, with
 459 care, to evaluate deep volatile inputs to the Rabaul volcanic-hydrothermal system, as described below.
 460 Likewise, $\delta^{13}C$ values of our gas samples from all localities extrapolate to values that are characteristic
 461 of magmatic arc fumaroles and provide information on CO_2 sources at Tavurvur.

462 5.2 Mantle versus crustal helium

463 We can use the air-corrected helium isotope composition of our samples to estimate the fraction of
 464 helium derived from the mantle beneath Rabaul rather than the crust, assuming a binary mixture of
 465 mantle and crustal end-members (Barry et al., 2013):

$$466 \text{ \% mantle helium} = (R_C/R_A - ^3He/^4He_{crust}) / (^3He/^4He_{mantle} - ^3He/^4He_{crust})$$

467 where $^3He/^4He_{mantle} = 8 R_A$ (Graham, 2002) and $^3He/^4He_{crust} = 0.05 R_A$ (Morrison and Pine, 1955).

468 Most of our Rabaul gases are characterised by 71 to 87 % mantle helium (13 to 29 % crustal helium),
 469 with the exception of the highly air contaminated sample from the Tavurvur crater floor, which has
 470 only 10 % mantle-derived helium (Table 2). The mean (\pm standard deviation) of 79 ± 5 % mantle helium
 471 for our non-contaminated samples is greater than the value of 67 % mantle helium in our sample from
 472 the Sulu Range hot springs at Silanga village, and lower than the values of 82 and 84 % (Garua Harbour)
 473 and 90 and 94 % (Garbuna) in our other New Britain volcanic gas samples (Table 2).

474 Mixing between primordial (mantle) and radiogenic (crustal) helium is typically controlled by crustal
 475 thickness (Barry et al., 2022; Hilton et al., 2002; Lages et al., 2021; Mason et al., 2017). Seismic
 476 refraction surveys suggest crustal thickness of ~ 32 km beneath Rabaul and the Gazelle Peninsula and

477 ~25 km under central New Britain and the Williaumez Peninsula (Finlayson et al., 1972). Our data are
 478 consistent with a small crustal influence beneath Rabaul and a lesser influence (higher R/R_A) in central
 479 New Britain where the crust is slightly thinner, i.e. beneath the Garua Harbour and Garbuna volcanic
 480 systems (Figure 3). The high R/R_A of 8.6 reported by Sano & Williams (1996) for Tavurvur was
 481 measured in gases emitted in an interval of relatively intense unrest, relative to our sampling periods,
 482 which may explain the stronger mantle (/magmatic) signature.

483 5.3 Sources of carbon

484 Figure 4 displays the $\delta^{13}\text{C}$ of fumarole and hot spring gases plotted against the inverse of CO_2
 485 concentration in each sample. We also show the carbon isotope composition of reference standards,
 486 (1) limestone, that is, subducted marine carbonate ($\delta^{13}\text{C} \sim 0 \text{ ‰}$) and (2) MORB, representing upper
 487 mantle material ($\delta^{13}\text{C} \sim -6.5 \pm 2.5$) (Sano and Marty, 1995). The majority of our data falls on a mixing
 488 line between air and a range in $\delta^{13}\text{C}$ that is intermediate between limestone and MORB (linear
 489 correlation coefficient of 0.86, y-intercept of -2.56 ± 0.62). The range in CO_2 and $\delta^{13}\text{C}$ exhibited by our
 490 samples indicates a variable degree of mixing between ambient air and deep fumarolic hot spring
 491 gases. A sample of pristine volcanic gas, that is, without any air contamination, would plot at the far
 492 left of this mixing line, close to the y-intercept. Thus, we can estimate the carbon isotopic composition
 493 of such a gas to be $\sim -2.6 \pm 0.62 \text{ ‰}$. This is isotopically high with respect to the upper mantle reservoir
 494 and would be consistent with CO_2 input from carbonate, either on the subducting slab or in the crustal
 495 country rocks. It closely matches the $\delta^{13}\text{C}$ values of -2.55 to -2.80 ‰ reported for Rabaul by Sano and
 496 Williams (1996).

497 Figure 5 displays the relative abundance of helium and CO_2 in our samples, together with their carbon
 498 isotope composition. Previous studies have established that He- CO_2 characteristics can also be used
 499 to determine relative mantle and subducted contributions (Halldórsson et al., 2013; Hilton et al., 2002;
 500 Mitchell et al., 2010; Sano and Marty, 1995; Sano and Williams, 1996; Snyder et al., 2001; van Soest
 501 et al., 1998). The method assumes that there is no crustal input of volatiles and that possible carbon
 502 reservoirs feeding volcanic outgassing are the mantle wedge (M), limestone (L) from subducted
 503 sediment or carbonate in the altered oceanic lithosphere, and sedimentary organic carbon (S). These
 504 reservoirs have distinct $\text{CO}_2/{}^3\text{He}$ ($M = 2 \times 10^9$, $L = 1 \times 10^{13}$, $S = 1 \times 10^{13}$) and $\delta^{13}\text{C}$ ($M = -5 \text{ ‰}$, $L = 0 \text{ ‰}$, S
 505 $= -30 \text{ ‰}$) as shown in Figure 5. Using the following equations (Sano and Marty, 1995), we can calculate
 506 the mass fraction of each potential source of carbon:

$$507 \quad ({}^{13}\text{C}/{}^{12}\text{C})_O = f_M({}^{13}\text{C}/{}^{12}\text{C})_M + f_L({}^{13}\text{C}/{}^{12}\text{C})_L + f_S({}^{13}\text{C}/{}^{12}\text{C})_S$$

$$508 \quad 1/({}^{12}\text{C}/{}^3\text{He})_O = f_M/({}^{12}\text{C}/{}^3\text{He})_M + f_L/({}^{12}\text{C}/{}^3\text{He})_L + f_S/({}^{12}\text{C}/{}^3\text{He})_S$$

$$509 \quad f_M + f_L + f_S = 1$$

510 where subscripts M, L, and S correspond to the mantle, limestone and sediment end members and
 511 subscript O is the measured or observed sample.

512 The mean L:S:M ratio we observe in our Rabaul samples is 59:14:27, though this is subject to large
 513 standard deviation (33:3:31) owing to our sample from the hot springs near Sulfur Point plotting close
 514 to the mantle range of $\delta^{13}\text{C}$ while our remaining samples plot close to the mixing line between mantle
 515 and limestone (Figure 5). The mean (and standard deviation) L:S:M ratio of the four Rababa hot spring
 516 and Tavurvur crater samples is 74:13:13 (10:2:10). The Sulfur Point hot springs sample is difficult to
 517 interpret: it has low R/R_A and ${}^4\text{He}/{}^{20}\text{Ne}$ consistent with substantial air contamination, yet higher He/Ar
 518 and N_2/Ar than any of our other Rabaul samples. This composition points to a dominance of slab over
 519 mantle in supplying carbon to Rabaul and, as above, suggests carbonates are the main carbon source,
 520 with a second, more modest input from organic sediments. This is reasonable, if the subducting

521 assemblage matches the calcareous mudstones and altered basalts sampled by dredging of the
522 Solomon sea floor (Crook, 1986; Davies and Price, 1986).

523 Sano & Marty (1995)'s approach assumes that only the mantle and the slab supply carbon to volcanic
524 emissions. Several studies have since argued that emissions from many volcanic arcs are subject to
525 substantial additions of carbon via the interaction of rising magmas and crustal carbonates (Barry et
526 al., 2022; Deegan et al., 2010; Lages et al., 2021; Mason et al., 2017; van Soest et al., 1998). Indeed,
527 Mason et al. (2017) identify PNG (not discriminating between New Britain, West Bismarck and
528 Bougainville) as one of a subset of arcs where outgassed carbon is sourced dominantly from crustal
529 limestone, along with Central America, the Aegean, Indonesia, Italy and parts of the Andes. Our data
530 suggests otherwise, with high air-corrected helium isotopes (R_C/R_A) in the majority of gas samples
531 pointing to only minimal crustal influence on outgassing. A minor role for crustal carbon is certainly
532 possible, given widespread growth of carbonate platforms across the region during the Miocene, but
533 we note that these rocks are most prevalent in the western part of the Gazelle Peninsula, separated
534 from Rabaul by major north-south trending fault systems, and may be unlikely as a result to influence
535 the magmatic system (Lindley, 2006; Madsen and Lindley, 1994).

536 **5.4 Sources of nitrogen**

537 Similarly to helium and carbon, we can quantitatively resolve the different contributions to Rabaul's
538 nitrogen output. Equations developed by (Sano et al., 2001, 1998) allow us to calculate how air (A),
539 upper mantle (M) and sediments (S) supply nitrogen to the volcanic system using measured $\delta^{15}\text{N}$ and
540 N_2/He values (Table 4, Figure 6):

$$541 \delta^{15}\text{N}_{\text{obs}} = (\delta^{15}\text{N}_A \times f_A) + (\delta^{15}\text{N}_M \times f_M) + (\delta^{15}\text{N}_S \times f_S)$$

$$542 1/(\text{N}_2/\text{He})_{\text{obs}} = f_A / (\text{N}_2/\text{He})_A + f_M / (\text{N}_2/\text{He})_M + f_S / (\text{N}_2/\text{He})_S$$

$$543 f_A + f_M + f_S = 1$$

544 where f_A , f_M , and f_S are the fractions of the measured N_2 derived from air, mantle and sediment
545 respectively and $\delta^{15}\text{N}_{A/M/S}$ and $\text{N}_2/\text{He}_{A/M/S}$ are the respective values of the end members. End member
546 $\delta^{15}\text{N}$ values are 0 ‰ for air, -5 ± 2 ‰ for the upper mantle, and $+7 \pm 4$ ‰ for sediments (Sano et al.,
547 2001). End member N_2/He values are 1.49×10^5 , 150, and 1.05×10^4 respectively (Fischer et al., 2002;
548 Sano et al., 2001).

549 Our samples from Tavurvur are likely to be subject to substantial air contamination, based on air-like
550 $\delta^{15}\text{N}$ (-0.75-1.99 ‰) and N_2/He in excess of 50,000. Our samples from Rababa show a range in $\delta^{15}\text{N}$ of
551 0.16-4.56 ‰ and so may provide more reliable insight into nitrogen sources. These isotopic values
552 suggest, a degree of atmospheric influence notwithstanding, that both upper mantle and subducted
553 organic sediments are supplying nitrogen to Rabaul's magma source region. Four of our five Rababa
554 samples appear to be subject to only limited air contamination and contain substantial (34-66%)
555 sediment-derived nitrogen. Following Mitchell et al. (2010), we calculate an air-corrected nitrogen
556 isotope composition, $\delta^{15}\text{N}_C$, that is:

$$557 \delta^{15}\text{N}_C = (\delta^{15}\text{N}_M \times f_M) + (\delta^{15}\text{N}_S \times (1 - f_M))$$

558 where $\delta^{15}\text{N}_M = -5$ ‰, $\delta^{15}\text{N}_S = +7$ ‰ and f_M is the fraction of mantle nitrogen derived above. We can
559 then calculate air-corrected contributions from sediment ($S_C = S/(S+M)$) and mantle ($M_C = 1 - S_C$). For
560 our four Rababa samples (little air contamination), S_C ranges from 96-98%, pointing to a dominantly
561 sedimentary over mantle origin for nitrogen. In summary, our $\delta^{15}\text{N}$ data, along with the $\delta^{13}\text{C}$ data
562 described above, indicate the influence of organic sediment on Rabaul volatiles. On the basis of high

563 $^3\text{He}/^4\text{He}$ in these gases, we judge the organic sediment influence to be sourced from the subducting
564 slab and not the result of assimilation of crustal volatiles.

565 **5.5 Volatile Provenance at Rabaul**

566 Our data allow, for the first time, an evaluation of the origins of magmatic volatiles and therefore
567 volcanic gases at Rabaul. Air-corrected helium isotope ratios, ranging from 5.7-6.9 R_C/R_A , are indicative
568 mantle-dominated helium and only minor crustal input. This is consistent with the relatively thin crust
569 beneath Rabaul and is characteristic of most intra-oceanic arcs (Hilton et al., 2002). Gas chemistry,
570 e.g. N_2/Ar and N_2/He , is also typical of arc volcanoes in low levels of unrest, indicating a mantle source
571 overprinted by slab influence and a degree of atmospheric contamination (Fischer, 2008).

572 Carbon isotopes, with $\delta^{13}\text{C}$ of pure magmatic CO_2 (i.e. a putative air-free sample) estimated at $\sim -2.6 \pm$
573 0.62 ‰ , suggest a mix of mantle, carbonate and organic sediment influences, with carbonate the
574 major source (75% in most samples). Based on our helium data, only minor volatiles can be supplied
575 from crustal rocks and hence we suggest a limited role for decarbonation of the Miocene Yalam
576 Formation limestones in supplying carbon to Rabaul. Instead, we favour the subducting slab as the
577 source of both carbonate- and organic sediment-derived CO_2 . The best estimates of the subducting
578 assemblage are provided by seafloor dredging only, and we emphasise caution is required in stating
579 that these unequivocally represent the slab lithologies. The calcareous mudrocks reported by Crook
580 (1986) are plausible sources of both carbonate and sedimentary carbon, and the altered basalts
581 described by Davies & Price (1986) are likely to be carbonate-bearing. Aiuppa et al. (2017) note that
582 the Solomon Sea depth and age make it likely that the seafloor has been above the carbonate
583 compensation depth for its entire history, which would support the idea of substantial carbonate flux
584 into the New Britain trench on the Solomon slab. Our data support the inference made by Aiuppa et
585 al. (2017, 2019) and subsequently by Plank & Manning (2019) that New Britain, and perhaps other arc
586 segments in PNG, are margins where carbon emissions are dominated by recycling of subducted
587 carbon. Further work is required to evaluate the relative importance of sedimentary carbonate versus
588 altered ocean crust or lithosphere. Thermodynamic modelling of the New Britain subduction zone
589 suggests that carbonate dissolution and metamorphic decarbonation of both sediments and altered
590 basalts are necessary to explain the volcanic arc carbon flux (Arzilli et al., 2023).

591 Our nitrogen isotope data, $\delta^{15}\text{N}$ of 0.16-4.56 ‰ in our least air-contaminated samples, further indicate
592 an influence of a second slab phase beyond carbonate, namely organic sediment. This fits with our
593 carbon isotope data and also the arguments advanced by Hohl et al. (2022) based on the whole-rock
594 geochemistry and isotope composition of Rabaul lavas. Further evidence for some organic sediment
595 involvement comes from our measurements of elevated $^{84}\text{Kr}/^{36}\text{Ar}$ and $^{132}\text{Xe}/^{36}\text{Ar}$ in our Rabaul hot
596 springs samples, i.e. those where heavy noble gas signatures deviate from atmospheric composition
597 (Supplementary Figure 1). We note that nitrogen isotopes in arc gases may be significantly influenced
598 by altered ocean crust, though given a lack of constraint on the variation of $\delta^{15}\text{N}$ through the Solomon
599 slab crust we have not attempted to evaluate this possibility quantitatively (c.f. Mitchell et al., 2010).

600 In summary, Rabaul volcanic gases are sourced from the mantle wedge with a substantial recycled
601 slab overprint that supplies carbon and nitrogen from carbonates, organic sediments, and potentially
602 altered ocean crust.

603

604 **6. Conclusion**

605 We have analysed the chemical and isotopic (He-C-N-Ne-Ar) composition of fumarole and hot spring
606 gases from Rabaul caldera, known to be among the most threatening and historically active volcanic
607 systems in Papua New Guinea, but one where activity has declined substantially over the last decade.
608 Ours is the first systematic study of gas composition to be undertaken at Rabaul and the first study to
609 explore volatile provenance at this volcano. Our gas samples are subject to variable and in some cases
610 overwhelming atmospheric contamination. Nonetheless, owing to our combination of helium (mantle
611 versus crust), carbon (mantle versus carbonate versus organic sediments) and nitrogen (mantle versus
612 organic sediments versus atmosphere) isotopic tracers we have been able to estimate the balance of
613 mantle, slab, and crustal influence on Rabaul volatiles.

614 Rabaul gases are comparable to those of other volcanic arcs, being enriched in carbon and nitrogen.
615 Helium isotopes point to a strong mantle rather than crustal influence, with air corrected He isotope
616 values ranging from 5.7-6.9 R_A and 71-87% of helium in Rabaul gases originating from the mantle.
617 Carbon isotopes ($\delta^{13}C$ estimated as -2.6 ± 0.62 ‰ for magmatic gases) indicate a combined mantle,
618 carbonate, and organic sediment influence, with slab carbonate providing the majority of carbon in
619 Rabaul gases. Nitrogen isotopes ($\delta^{15}N \sim 0.16$ -4.56 ‰ in our least air-contaminated samples) also point
620 to a second sedimentary source, organic sediments. We consider both carbonate and sedimentary
621 influences to originate from the nearby subducting Solomon Sea slab, though minor crustal
622 contributions are plausible, especially of carbonate.

623 Many characteristics of the Rabaul volcanic system remain little explored and our understanding of
624 volatile provenance in the New Britain arc is at a nascent stage. In this contribution, our focus is to
625 determine the reservoirs feeding outgassing from the Rabaul caldera complex, and we conclude that
626 the nearby subducting slab plays a significant role in augmenting volatile supply from the upper mantle
627 reservoir beneath Rabaul. Future work should investigate whether the high outgassing of the 1994-
628 2014 eruptive interval is characteristic of the long-term behaviour of Rabaul or not, and whether
629 Rabaul magmas are notably volatile-rich. There remain major unknowns in the wider regional
630 geological context, including an absence of core samples of the subducting lithologies and the relative
631 influence of both ongoing (New Britain trench) and earlier (Vitiiaz-Melanesian trench) sequences of
632 subduction recycling on the mantle wedge below the Bismarck Sea and Manus Basin.

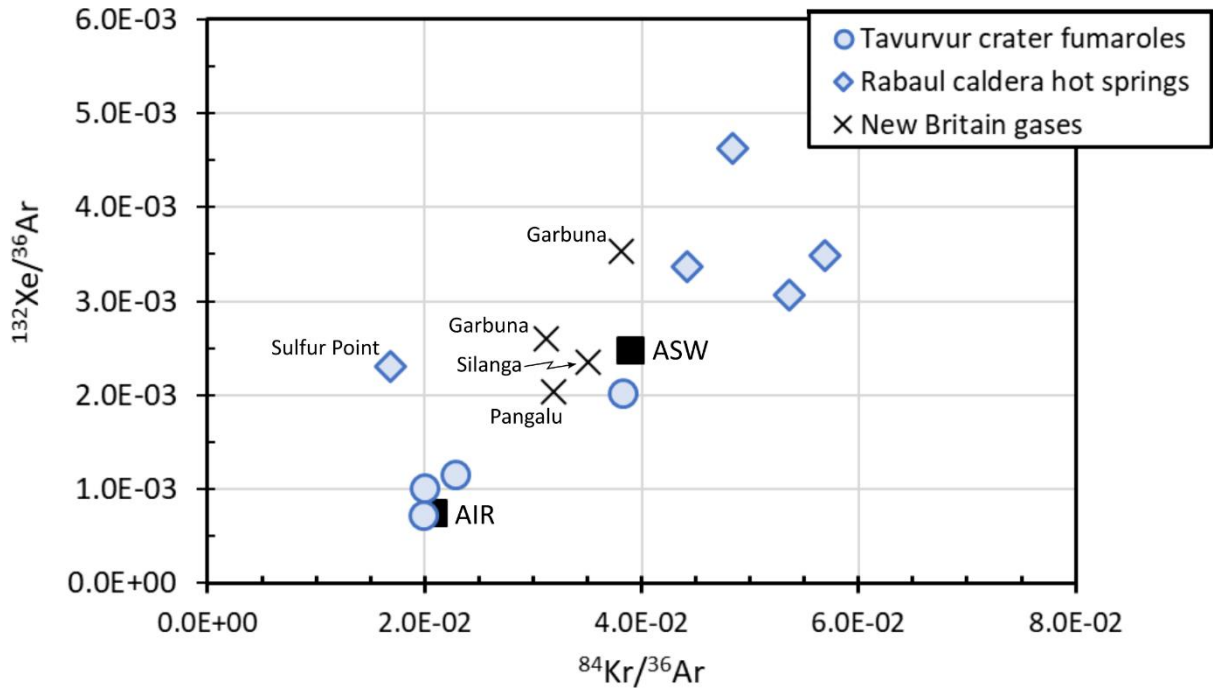
633

634 **Acknowledgements**

635 We acknowledge financial support of the Alfred P Sloan foundation, awarded via the Deep Carbon
636 Observatory, specifically the Deep Earth Degassing (DECADE) programme of the Reservoirs and
637 Fluxes division. BMK acknowledges a travel grant from the NERC Centre for Observation and
638 Modelling of Earthquakes, Volcanoes and Tectonics which supported an early visit to Rabaul. We are
639 grateful to the Tolai communities of Rabaul, especially Matupit for their support in accessing the
640 field sites and for valuable conversations about past and recent volcanic unrest.

641

642



643 **Supplementary Figure 1.** Heavy noble gases in a subset of our samples (those analysed at University
 644 of Oxford in 2016 and University of Manchester in 2019). $^{84}\text{Kr}/^{36}\text{Ar}$ and $^{132}\text{Xe}/^{36}\text{Ar}$ in air and air-
 645 saturated water after Ozima and Podisek (2001).

646 **References**

- 647 Aiuppa, A., Fischer, T.P., Plank, T., Bani, P., 2019. CO₂ flux emissions from the Earth's most actively
648 degassing volcanoes, 2005–2015. *Sci. Rep.* 9, 1–17. [https://doi.org/10.1038/s41598-019-](https://doi.org/10.1038/s41598-019-41901-y)
649 [41901-y](https://doi.org/10.1038/s41598-019-41901-y)
- 650 Aiuppa, A., Fischer, T.P., Plank, T., Robidoux, P., Di Napoli, R., 2017. Along-arc, inter-arc and arc-to-
651 arc variations in volcanic gas CO₂/ST ratios reveal dual source of carbon in arc volcanism.
652 *Earth-Sci. Rev.* 168, 24–47. <https://doi.org/10.1016/j.earscirev.2017.03.005>
- 653 Andres, R., Kasgnoc, A., 1998. A time-averaged inventory of subaerial volcanic sulfur emissions. *J.*
654 *Geophys. Res. Atmospheres* 103, 25251–25261. <https://doi.org/10.1029/98JD02091>
- 655 Andrews, J.N., 1985. The isotopic composition of radiogenic helium and its use to study groundwater
656 movement in confined aquifers. *Chem. Geol., Water-Rock Interaction* 49, 339–351.
657 [https://doi.org/10.1016/0009-2541\(85\)90166-4](https://doi.org/10.1016/0009-2541(85)90166-4)
- 658 Arzilli, F., Burton, M., La Spina, G., Macpherson, C.G., van Keken, P.E., McCann, J., 2023.
659 Decarbonation of subducting carbonate-bearing sediments and basalts of altered oceanic
660 crust: Insights into recycling of CO₂ through volcanic arcs. *Earth Planet. Sci. Lett.* 602,
661 117945. <https://doi.org/10.1016/j.epsl.2022.117945>
- 662 Barry, P.H., Bekaert, D.V., Krantz, J.A., Halldórsson, S.A., de Moor, J.M., Fischer, T.P., Werner, C.,
663 Kelly, P.J., Seltzer, A.M., Franz, B.P., Kulongoski, J.T., 2021. Helium-carbon systematics of
664 groundwaters in the Lassen Peak Region. *Chem. Geol.* 584, 120535.
665 <https://doi.org/10.1016/j.chemgeo.2021.120535>
- 666 Barry, P.H., De Moor, J.M., Chiodi, A., Aguilera, F., Hudak, M.R., Bekaert, D.V., Turner, S.J., Curtice, J.,
667 Seltzer, A.M., Jessen, G.L., Osses, E., Blamey, J.M., Amenábar, M.J., Selci, M., Cascone, M.,
668 Bastianoni, A., Nakagawa, M., Filipovich, R., Bustos, E., Schrenk, M.O., Buongiorno, J.,
669 Ramírez, C.J., Rogers, T.J., Lloyd, K.G., Giovannelli, D., 2022. The Helium and Carbon Isotope
670 Characteristics of the Andean Convergent Margin. *Front. Earth Sci.* 10.
- 671 Barry, P.H., Hilton, D.R., Fischer, T.P., de Moor, J.M., Mangasini, F., Ramirez, C., 2013. Helium and
672 carbon isotope systematics of cold “mazuku” CO₂ vents and hydrothermal gases and fluids
673 from Rungwe Volcanic Province, southern Tanzania. *Chem. Geol., Frontiers in Gas*
674 *Geochemistry* 339, 141–156. <https://doi.org/10.1016/j.chemgeo.2012.07.003>
- 675 Barry, P.H., Hilton, D.R., Halldórsson, S.A., Hahm, D., Marti, K., 2012. High precision nitrogen isotope
676 measurements in oceanic basalts using a static triple collection noble gas mass
677 spectrometer. *Geochem. Geophys. Geosystems* 13. <https://doi.org/10.1029/2011GC003878>
- 678 Barry, P.H., Lawson, M., Meurer, W.P., Warr, O., Mabry, J.C., Byrne, D.J., Ballentine, C.J., 2016. Noble
679 gases solubility models of hydrocarbon charge mechanism in the Sleipner Vest gas field.
680 *Geochim. Cosmochim. Acta* 194, 291–309. <https://doi.org/10.1016/j.gca.2016.08.021>
- 681 Bekaert, D.V., Barry, P.H., Broadley, M.W., 2023. Carbon, nitrogen, and multi-isotope study of upper
682 mantle geochemical heterogeneities near 14°N on the Mid-Atlantic Ridge. *Geochim.*
683 *Cosmochim. Acta.*
- 684 Bekaert, D.V., Turner, S.J., Broadley, M.W., Barnes, J.D., Halldórsson, S.A., Labidi, J., Wade, J.,
685 Walowski, K.J., Barry, P.H., 2021. Subduction-Driven Volatile Recycling: A Global Mass
686 Balance. *Annu. Rev. Earth Planet. Sci.* 49, 37–70. [https://doi.org/10.1146/annurev-earth-](https://doi.org/10.1146/annurev-earth-071620-055024)
687 [071620-055024](https://doi.org/10.1146/annurev-earth-071620-055024)
- 688 Bernard, O., Bouvet de Maisonneuve, C., 2020. Controls on eruption style at Rabaul, Papua New
689 Guinea – Insights from microlites, porosity and permeability measurements. *J. Volcanol.*
690 *Geotherm. Res.* 406. <https://doi.org/10.1016/j.jvolgeores.2020.107068>
- 691 Bernard, O., Li, W., Costa, F., Saunders, S., Itikarai, I., Sindang, M., Bouvet de Maisonneuve, C., 2022.
692 Explosive-effusive-explosive: The role of magma ascent rates and paths in modulating
693 caldera eruptions. *Geology* 50, 1013–1017. <https://doi.org/10.1130/G50023.1>
- 694 Bernstein-Taylor, B.L., Kirchoff-Stein, K.S., Silver, E.A., Reed, D.L., Mackay, M., 1992. Large-scale
695 duplexes within the New Britain Accretionary Wedge: A possible example of accreted
696 ophiolitic slivers. *Tectonics* 11, 732–752. <https://doi.org/10.1029/91TC02901>

- 697 Bouvet de Maisonneuve, C., Costa, F., Patia, H., Huber, C., 2015. Mafic magma replenishment, unrest
698 and eruption in a caldera setting: Insights from the 2006 eruption of Rabaul (Papua New
699 Guinea), Geological Society Special Publication. <https://doi.org/10.1144/SP422.2>
- 700 Broadley, M.W., Barry, P.H., Bekaert, D.V., Byrne, D.J., Caracausi, A., Ballentine, C.J., Marty, B., 2020.
701 Identification of chondritic krypton and xenon in Yellowstone gases and the timing of
702 terrestrial volatile accretion. *Proc. Natl. Acad. Sci.* 117, 13997–14004.
703 <https://doi.org/10.1073/pnas.2003907117>
- 704 Carn, S.A., Clarisse, L., Prata, A.J., 2016. Multi-decadal satellite measurements of global volcanic
705 degassing. *J. Volcanol. Geotherm. Res.* 311, 99–134.
706 <https://doi.org/10.1016/j.jvolgeores.2016.01.002>
- 707 Carn, S.A., Fioletov, V.E., McLinden, C.A., Li, C., Krotkov, N.A., 2017. A decade of global volcanic SO₂
708 emissions measured from space. *Sci. Rep.* 7, 1–12. <https://doi.org/10.1038/srep44095>
- 709 Clor, L.E., Fischer, T.P., Hilton, D.R., Sharp, Z.D., Hartono, U., 2005. Volatile and N isotope chemistry
710 of the Molucca Sea collision zone: Tracing source components along the Sangihe Arc,
711 Indonesia. *Geochem. Geophys. Geosystems* 6. <https://doi.org/10.1029/2004GC000825>
- 712 Craig, H., Poreda, R.J., 1987. Studies of methane and helium in hydrothermal vent plumes,
713 spreading-axis basalts and volcanic island lavas and gases in Southwest Pacific marginal
714 basins, Scripps Institution of Oceanography.
- 715 Crook, K.A.W., 1986. Petrology and mineral chemistry of sedimentary rocks from the Western
716 Solomon Sea. *Geo-Mar. Lett.* 6, 203–209. <https://doi.org/10.1007/BF02239581>
- 717 Davies, H.L., Price, R.C., 1986. Basalts from the Solomon and Bismarck Seas. *Geo-Mar. Lett.* 6, 193–
718 202. <https://doi.org/10.1007/BF02239580>
- 719 Deegan, F.M., Troll, V.R., Freda, C., Misiti, V., Chadwick, J.P., McLeod, C.L., Davidson, J.P., 2010.
720 Magma–Carbonate Interaction Processes and Associated CO₂ Release at Merapi Volcano,
721 Indonesia: Insights from Experimental Petrology. *J. Petrol.* 51, 1027–1051.
722 <https://doi.org/10.1093/petrology/egq010>
- 723 DePaolo, D.J., Johnson, R.W., 1979. Magma genesis in the New Britain island-arc: Constraints from
724 Nd and Sr isotopes and trace-element patterns. *Contrib. Mineral. Petrol.* 70, 367–379.
725 <https://doi.org/10.1007/BF00371044>
- 726 Fabbro, G.N., McKee, C.O., Sindang, M.E., Eggins, S., Bouvet de Maisonneuve, C., 2020. Variable
727 mafic recharge across a caldera cycle at Rabaul, Papua New Guinea. *J. Volcanol. Geotherm.*
728 *Res.* 393, 106810. <https://doi.org/10.1016/j.jvolgeores.2020.106810>
- 729 Farley, K.A., Patterson, D., McInnes, B., 1995. He-isotopic investigation of geothermal gases from the
730 Tabar-Lihir-Tanga-Feni arc and Rabaul, Papua New Guinea. *AIP Conf. Proc.* 341, 81–90.
731 <https://doi.org/10.1063/1.48752>
- 732 Finlayson, D.M., Cull, J.P., Wiebenga, W.A., Furumoto, A.S., Webb, J.P., 1972. New Britain—New
733 Ireland Crustal Seismic Refraction Investigations 1967 and 1969. *Geophys. J. Int.* 29, 245–
734 253. <https://doi.org/10.1111/j.1365-246X.1972.tb06157.x>
- 735 Fischer, T.P., 2008. Fluxes of volatiles (H₂O, CO₂, N₂, Cl, F) from arc volcanoes. *Geochem. J.* 42, 21–38.
736 <https://doi.org/10.2343/geochemj.42.21>
- 737 Fischer, T.P., Arellano, S., Carn, S., Aiuppa, A., Galle, B., Allard, P., Lopez, T., Shinohara, H., Kelly, P.,
738 Werner, C., Cardellini, C., Chiodini, G., 2019. The emissions of CO₂ and other volatiles from
739 the world's subaerial volcanoes. *Sci. Rep.* 9, 18716. <https://doi.org/10.1038/s41598-019-54682-1>
- 740
- 741 Fischer, T.P., Giggenbach, W.F., Sano, Y., Williams, S.N., 1998. Fluxes and sources of volatiles
742 discharged from Kudryavy, a subduction zone volcano, Kurile Islands. *Earth Planet. Sci. Lett.*
743 160, 81–96. [https://doi.org/10.1016/S0012-821X\(98\)00086-7](https://doi.org/10.1016/S0012-821X(98)00086-7)
- 744 Fischer, T.P., Hilton, D.R., Zimmer, M.M., Shaw, A.M., Sharp, Z.D., Walker, J.A., 2002. Subduction and
745 Recycling of Nitrogen Along the Central American Margin. *Science* 297, 1154–1157.
746 <https://doi.org/10.1126/science.1073995>

- 747 Fischer, T.P., Lopez, T.M., 2016. First airborne samples of a volcanic plume for $\delta^{13}\text{C}$ of CO_2
748 determinations. *Geophys. Res. Lett.* 43, 3272–3279. <https://doi.org/10.1002/2016GL068499>
- 749 Fischer, T.P., Lopez, T.M., Aiuppa, A., Rizzo, A.L., Ilanko, T., Kelley, K.A., Cottrell, E., 2021. Gas
750 Emissions From the Western Aleutians Volcanic Arc. *Front. Earth Sci.* 9.
- 751 Fischer, T.P., Takahata, N., Sano, Y., Sumino, H., Hilton, D.R., 2005. Nitrogen isotopes of the mantle:
752 Insights from mineral separates. *Geophys. Res. Lett.* 32, 1–5.
753 <https://doi.org/10.1029/2005GL022792>
- 754 Galewsky, J., Silver, E.A., 1997. Tectonic controls on facies transitions in an oblique collision: The
755 western Solomon Sea, Papua New Guinea. *GSA Bull.* 109, 1266–1278.
756 [https://doi.org/10.1130/0016-7606\(1997\)109<1266:TCOFTI>2.3.CO;2](https://doi.org/10.1130/0016-7606(1997)109<1266:TCOFTI>2.3.CO;2)
- 757 Galle, B., Arellano, S., Bobrowski, N., Conde, V., Fischer, T.P., Gerdes, G., Gutmann, A., Hoffmann, T.,
758 Itikarai, I., Krejci, T., Liu, E.J., Mulina, K., Nowicki, S., Richardson, T., Rüdiger, J., Wood, K., Xu,
759 J., 2021. A multi-purpose, multi-rotor drone system for long-range and high-altitude volcanic
760 gas plume measurements. *Atmospheric Meas. Tech.* 14, 4255–4277.
761 <https://doi.org/10.5194/amt-14-4255-2021>
- 762 Giggenbach, W.F., 1975. A simple method for the collection and analysis of volcanic gas samples.
763 *Bull. Volcanol.* 39, 132–145. <https://doi.org/10.1007/BF02596953>
- 764 Giggenbach, W.F., Goguel, R.L., 1989. Methods for the Collection and Analysis of Geothermal and
765 Volcanic Water and Gas Samples. Chemistry Division, Department of Scientific and Industrial
766 Research.
- 767 Global Volcanism Program, 2013. *Volcanoes of the World [WWW Document]*. V 4110 08 Jun 2022.
768 URL <https://volcano.si.edu/> (accessed 6.30.22).
- 769 Global Volcanism Program, 1997a. Global Volcanism Program | Report on Rabaul (Papua New
770 Guinea) — November 1997 22.
- 771 Global Volcanism Program, 1997b. Global Volcanism Program | Report on Rabaul (Papua New
772 Guinea) — December 1997 22.
- 773 Global Volcanism Program, 1995. Report on Rabaul (Papua New Guinea) — December 1995. *Bull.*
774 *Glob. Volcanism Netw.* 20.
- 775 Graham, D.W., 2002. Noble Gas Isotope Geochemistry of Mid-Ocean Ridge and Ocean Island Basalts:
776 Characterization of Mantle Source Reservoirs. *Rev. Mineral. Geochem.* 47, 247–317.
777 <https://doi.org/10.2138/rmg.2002.47.8>
- 778 Halldórsson, S.A., Hilton, D.R., Troll, V.R., Fischer, T.P., 2013. Resolving volatile sources along the
779 western Sunda arc, Indonesia. *Chem. Geol.* 339, 263–282.
780 <https://doi.org/10.1016/j.chemgeo.2012.09.042>
- 781 Heming, R.F., 1974. Geology and petrology of Rabaul Caldera, Papua New Guinea. *Bull. Geol. Soc.*
782 *Am.* 85, 1253–1264. [https://doi.org/10.1130/0016-7606\(1974\)85<1253:GAPORC>2.0.CO;2](https://doi.org/10.1130/0016-7606(1974)85<1253:GAPORC>2.0.CO;2)
- 783 Hilton, D.R., 1996. The helium and carbon isotope systematics of a continental geothermal system:
784 results from monitoring studies at Long Valley caldera (California, U.S.A.). *Chem. Geol.* 127,
785 269–295. [https://doi.org/10.1016/0009-2541\(95\)00134-4](https://doi.org/10.1016/0009-2541(95)00134-4)
- 786 Hilton, D.R., Fischer, T.P., Marty, B., 2002. Noble Gases and Volatile Recycling at Subduction Zones.
787 *Rev. Mineral. Geochem.* 47, 319–370. <https://doi.org/10.2138/rmg.2002.47.9>
- 788 Hohl, S.V., Schuth, S., Münker, C., König, S., Garbe-Schönberg, D., Kuduon, J., 2022. Geochemical
789 evolution of the Rabaul volcanic complex, Papua New Guinea - Insights from HFSE, Sr-Nd-Hf,
790 and Fe isotopes. *Lithos* 408–409, 106560. <https://doi.org/10.1016/j.lithos.2021.106560>
- 791 Holm, R.J., Rosenbaum, G., Richards, S.W., 2016. Post 8Ma reconstruction of Papua New Guinea and
792 Solomon Islands: Microplate tectonics in a convergent plate boundary setting. *Earth-Sci. Rev.*
793 156, 66–81. <https://doi.org/10.1016/j.earscirev.2016.03.005>
- 794 Honza, E., Miyazaki, T., Lock, J., 1989. Subduction erosion and accretion in the Solomon Sea region.
795 *Tectonophysics, Subduction Zones: The Kaiko Project* 160, 49–62.
796 [https://doi.org/10.1016/0040-1951\(89\)90383-1](https://doi.org/10.1016/0040-1951(89)90383-1)

- 797 Ilanko, T., Fischer, T.P., Kyle, P., Curtis, A., Lee, H., Sano, Y., 2019. Modification of fumarolic gases by
798 the ice-covered edifice of Erebus volcano, Antarctica. *J. Volcanol. Geotherm. Res.* 381, 119–
799 139. <https://doi.org/10.1016/j.jvolgeores.2019.05.017>
- 800 Jambon, A., 1994. Earth degassing and large-scale geochemical cycling of volatile elements. *Rev.*
801 *Mineral. Geochem.* 30, 479–517.
- 802 Johnson, R.W., 1979. Geotectonics and volcanism in Papua New Guinea: a review of the late
803 Cainozoic. *BMR J. Aust. Geol. Geophys.* 4, 181–207.
- 804 Johnson, R.W., McKee, C.O., Eggins, S., Woodhead, J.D., Arculus, R.J., Chappell, B.W., Sheraton, J.,
805 1995. Taking petrologic pathways toward understanding Rabaul's restless caldera. *Eos Trans.*
806 *Am. Geophys. Union* 76, 171–180. <https://doi.org/10.1029/95EO00093>
- 807 Joshima, M., Honza, E., 1986. Age estimation of the Solomon Sea based on heat flow data. *Geo-Mar.*
808 *Lett.* 6, 211–217. <https://doi.org/10.1007/BF02239582>
- 809 Joshima, M., Okuda, Y., Murakami, F., Kishimoto, K., Honza, E., 1986. Age of the Solomon Sea Basin
810 from magnetic lineations. *Geo-Mar. Lett.* 6, 229–234. <https://doi.org/10.1007/BF02239584>
- 811 Kagoshima, T., Sano, Y., Takahata, N., Maruoka, T., Fischer, T.P., Hattori, K., 2015. Sulphur
812 geodynamic cycle. *Sci. Rep.* 5, 8330. <https://doi.org/10.1038/srep08330>
- 813 Keeling, C.D., 1958. The concentration and isotopic abundances of atmospheric carbon dioxide in
814 rural areas. *Geochim. Cosmochim. Acta* 13, 322–334. [https://doi.org/10.1016/0016-](https://doi.org/10.1016/0016-7037(58)90033-4)
815 [7037\(58\)90033-4](https://doi.org/10.1016/0016-7037(58)90033-4)
- 816 Lages, J., Rizzo, A.L., Aiuppa, A., Samaniego, P., Le Pennec, J.L., Ceballos, J.A., Narváez, P.A.,
817 Moussallam, Y., Bani, P., Schipper, C.I., Hidalgo, S., Gaglio, V., Alberti, E., Sandoval-Velasquez,
818 A., 2021. Noble gas magmatic signature of the Andean Northern Volcanic Zone from fluid
819 inclusions in minerals. *Chem. Geol.* 559, 119966.
820 <https://doi.org/10.1016/j.chemgeo.2020.119966>
- 821 Lee, H., Fischer, T.P., Muirhead, J.D., Ebinger, C.J., Kattenhorn, S.A., Sharp, Z.D., Kianji, G., Takahata,
822 N., Sano, Y., 2017. Incipient rifting accompanied by the release of subcontinental
823 lithospheric mantle volatiles in the Magadi and Natron basin, East Africa. *J. Volcanol.*
824 *Geotherm. Res., Volcano-Hydrothermal Systems* 346, 118–133.
825 <https://doi.org/10.1016/j.jvolgeores.2017.03.017>
- 826 Lee, J.-Y., Marti, K., Severinghaus, J.P., Kawamura, K., Yoo, H.-S., Lee, J.B., Kim, J.S., 2006. A
827 redetermination of the isotopic abundances of atmospheric Ar. *Geochim. Cosmochim. Acta*
828 70, 4507–4512. <https://doi.org/10.1016/j.gca.2006.06.1563>
- 829 Lindley, I., 2006. Extensional and vertical tectonics in the New Guinea islands: Implications for island
830 arc evolution. *Ann. Geophys.* 49.
- 831 Liu, E.J., Aiuppa, A., Alan, A., Arellano, S., Bitetto, M., Bobrowski, N., Carn, S., Clarke, R., Corrales, E.,
832 de Moor, J.M., Diaz, J.A., Edmonds, M., Fischer, T.P., Freer, J., Fricke, G.M., Galle, B., Gerdes,
833 G., Giudice, G., Gutmann, A., Hayer, C., Itikarai, I., Jones, J., Mason, E., McCormick Kilbride,
834 B.T., Mulina, K., Nowicki, S., Rahilly, K., Richardson, T., Rüdiger, J., Schipper, C.I., Watson,
835 I.M., Wood, K., 2020. Aerial strategies advance volcanic gas measurements at inaccessible,
836 strongly degassing volcanoes. *Sci. Adv.* 6, eabb9103.
837 <https://doi.org/10.1126/sciadv.abb9103>
- 838 Macpherson, C.G., Hilton, D.R., Sinton, J.M., Poreda, R.J., Craig, H., 1998. High $^3\text{He}/^4\text{He}$ ratios in the
839 Manus backarc basin: Implications for mantle mixing and the origin of plumes in the western
840 Pacific Ocean. *Geology* 26, 1007–1010. [https://doi.org/10.1130/0091-](https://doi.org/10.1130/0091-7613(1998)026<1007:HHHRIT>2.3.CO;2)
841 [7613\(1998\)026<1007:HHHRIT>2.3.CO;2](https://doi.org/10.1130/0091-7613(1998)026<1007:HHHRIT>2.3.CO;2)
- 842 Madsen, J.A., Lindley, I.D., 1994. Large-scale structures on Gazelle Peninsula, New Britain:
843 Implications for the evolution of the New Britain arc. *Aust. J. Earth Sci.* 41, 561–569.
844 <https://doi.org/10.1080/08120099408728166>
- 845 Malatesta, C., Gerya, T., Crispini, L., Federico, L., Capponi, G., 2013. Oblique subduction modelling
846 indicates along-trench tectonic transport of sediments. *Nat. Commun.* 4, 2456.
847 <https://doi.org/10.1038/ncomms3456>

- 848 Marty, B., Almayrac, M., Barry, P.H., Bekaert, D.V., Broadley, M.W., Byrne, D.J., Ballentine, C.J.,
849 Caracausi, A., 2020. An evaluation of the C/N ratio of the mantle from natural CO₂-rich gas
850 analysis: Geochemical and cosmochemical implications. *Earth Planet. Sci. Lett.* 551, 116574.
851 <https://doi.org/10.1016/j.epsl.2020.116574>
- 852 Mason, E., Edmonds, M., Turchyn, A.V., 2017. Remobilization of crustal carbon may dominate
853 volcanic arc emissions. *Science* 357, 290–294. <https://doi.org/10.1126/science.aan5049>
- 854 McCormick, B.T., Edmonds, M., Mather, T.A., Carn, S.A., 2012. First synoptic analysis of volcanic
855 degassing in Papua New Guinea. *Geochem. Geophys. Geosystems* 13.
856 <https://doi.org/10.1029/2011GC003945>
- 857 McCormick Kilbride, B.T., Nicholson, E.J., Wood, K.T., Wilkes, T.C.S., Schipper, C.I., Mulina, K., Itikarai,
858 I., Richardson, T., Werner, C., Hayer, C.S.L., Esse, B., Burton, M., Pering, T.D., McGonigle,
859 A.J.S., Coppola, D., Bitetto, M., Giudice, G., Aiuppa, A., 2023. Temporal Variability in Gas
860 Emissions at Bagana Volcano Revealed by Aerial, Ground, and Satellite Observations.
861 *Geochem. Geophys. Geosystems*.
- 862 McGonigle, A.J.S., Oppenheimer, C., Tsanev, V.I., Saunders, S., Mulina, K., Tohui, S., Bosco, J., Nahou,
863 J., Kuduon, J., Taranu, F., 2004. Sulphur dioxide fluxes from Papua New Guinea's volcanoes.
864 *Geophys. Res. Lett.* 31. <https://doi.org/10.1029/2004GL019568>
- 865 McKee, C.O., Baillie, M.G., Reimer, P.J., 2015. A revised age of ad 667–699 for the latest major
866 eruption at Rabaul. *Bull. Volcanol.* 77. <https://doi.org/10.1007/s00445-015-0954-7>
- 867 Mitchell, E.C., Fischer, T.P., Hilton, D.R., Hauri, E.H., Shaw, A.M., De Moor, J.M., Sharp, Z.D.,
868 Kazahaya, K., 2010. Nitrogen sources and recycling at subduction zones: Insights from the
869 Izu-Bonin-Mariana arc. *Geochem. Geophys. Geosystems* 11.
870 <https://doi.org/10.1029/2009GC002783>
- 871 Morris, J.D., Leeman, W.P., Tera, F., 1990. The subducted component in island arc lavas: constraints
872 from Be isotopes and B–Be systematics. *Nature* 344, 31–36.
873 <https://doi.org/10.1038/344031a0>
- 874 Morrison, P., Pine, J., 1955. Radiogenic Origin of the Helium Isotopes in Rock. *Ann. N. Y. Acad. Sci.* 62,
875 71–92. <https://doi.org/10.1111/j.1749-6632.1955.tb35366.x>
- 876 Nairn, I.A., McKee, C.O., Talai, B., Wood, C.P., 1995. Geology and eruptive history of the Rabaul
877 Caldera area, Papua New Guinea. *J. Volcanol. Geotherm. Res.* 69, 255–284.
878 [https://doi.org/10.1016/0377-0273\(95\)00035-6](https://doi.org/10.1016/0377-0273(95)00035-6)
- 879 Ozima, M., Podosek, F.A., 2002. *Noble Gas Geochemistry*, 2nd ed. Cambridge University Press,
880 Cambridge. <https://doi.org/10.1017/CBO9780511545986>
- 881 Patia, H., Eggins, S.M., Arculus, R.J., McKee, C.O., Johnson, R.W., Bradney, A., 2017. The 1994–2001
882 eruptive period at Rabaul, Papua New Guinea: Petrological and geochemical evidence for
883 basalt injections into a shallow dacite magma reservoir, and significant SO₂ flux. *J. Volcanol.*
884 *Geotherm. Res.* 345, 200–217. <https://doi.org/10.1016/j.jvolgeores.2017.08.011>
- 885 Plank, T., Manning, C.E., 2019. Subducting carbon. *Nature* 574, 343–352.
886 <https://doi.org/10.1038/s41586-019-1643-z>
- 887 Sano, Y., Marty, B., 1995. Origin of carbon in fumarolic gas from island arcs. *Chem. Geol.* 119, 265–
888 274. [https://doi.org/10.1016/0009-2541\(94\)00097-R](https://doi.org/10.1016/0009-2541(94)00097-R)
- 889 Sano, Y., Takahata, N., Nishio, Y., Fischer, T.P., Williams, S.N., 2001. Volcanic flux of nitrogen from the
890 Earth. *Chem. Geol.* 171, 263–271. [https://doi.org/10.1016/S0009-2541\(00\)00252-7](https://doi.org/10.1016/S0009-2541(00)00252-7)
- 891 Sano, Y., Takahata, N., Nishio, Y., Marty, B., 1998. Nitrogen recycling in subduction zones. *Geophys.*
892 *Res. Lett.* 25, 2289–2292. <https://doi.org/10.1029/98GL01687>
- 893 Sano, Y., Williams, S.N., 1996. Fluxes of mantle and subducted carbon along convergent plate
894 boundaries. *Geophys. Res. Lett.* 23, 2749–2752. <https://doi.org/10.1029/96GL02260>
- 895 Snyder, G., Poreda, R., Hunt, A., Fehn, U., 2001. Regional variations in volatile composition: Isotopic
896 evidence for carbonate recycling in the Central American volcanic arc. *Geochem. Geophys.*
897 *Geosystems* 2. <https://doi.org/10.1029/2001GC000163>

- 898 Syracuse, E.M., Abers, G.A., 2006. Global compilation of variations in slab depth beneath arc
899 volcanoes and implications. *Geochem. Geophys. Geosystems* 7.
900 <https://doi.org/10.1029/2005GC001045>
- 901 Tregoning, P., Lambeck, K., Stolz, A., Morgan, P., McClusky, S.C., van der Beek, P., McQueen, H.,
902 Jackson, R.J., Little, R.P., Laing, A., Murphy, B., 1998. Estimation of current plate motions in
903 Papua New Guinea from Global Positioning System observations. *J. Geophys. Res. Solid Earth*
904 103, 12181–12203. <https://doi.org/10.1029/97JB03676>
- 905 Tregoning, P., McQueen, H., Lambeck, K., Jackson, R., Little, R., Saunders, S., Rosa, R., 2000. Present-
906 day crustal motion in Papua New Guinea. *Earth Planets Space* 52, 727–730.
907 <https://doi.org/10.1186/BF03352272>
- 908 van Soest, M.C., Hilton, D.R., Kreulen, R., 1998. Tracing crustal and slab contributions to arc
909 magmatism in the lesser antilles island arc using helium and carbon relationships in
910 geothermal fluids. *Geochim. Cosmochim. Acta* 62, 3323–3335.
911 [https://doi.org/10.1016/S0016-7037\(98\)00241-5](https://doi.org/10.1016/S0016-7037(98)00241-5)
- 912 Wood, C.P., Nairn, I.A., Mckee, C.O., Talai, B., 1995. Petrology of the Rabaul Caldera area, Papua New
913 Guinea. *J. Volcanol. Geotherm. Res.* 69, 285–302. [https://doi.org/10.1016/0377-](https://doi.org/10.1016/0377-0273(95)00034-8)
914 [0273\(95\)00034-8](https://doi.org/10.1016/0377-0273(95)00034-8)
- 915 Woodhead, J.D., Eggins, S.M., Johnson, R.W., 1998. Magma Genesis in the New Britain Island Arc:
916 Further Insights into Melting and Mass Transfer Processes. *J. Petrol.* 39, 1641–1668.
917 <https://doi.org/10.1093/petroj/39.9.1641>
- 918 Woodhead, J.D., Johnson, R.W., 1993. Isotopic and trace-element profiles across the New Britain
919 island arc, Papua New Guinea. *Contrib. Mineral. Petrol.* 113, 479–491.
920 <https://doi.org/10.1007/BF00698317>
- 921 Zhang, H., Gong, W., Xing, J., Xu, C., Li, C., 2023. The Subduction Structure Beneath the New Britain
922 Island Arc and the Adjacent Region from Double-Difference Tomography. *J. Ocean Univ.*
923 *China* 22, 107–118. <https://doi.org/10.1007/s11802-023-5282-5>
924